

## Supporting Information

### Stereoselective Ring-Opening Polymerization of Functional $\beta$ -Lactones: Influence of the Exocyclic Side-Group †

Rama M. Shakaroun,<sup>a,b,‡</sup> Hui Li,<sup>a,‡</sup> Philippe Jéhan,<sup>c</sup> Marielle Blot,<sup>a</sup> Ali Alaaeddine,<sup>b</sup> Jean-François Carpentier,\*<sup>a</sup> and Sophie M. Guillaume\*<sup>a</sup>

<sup>a</sup> Univ. Rennes, CNRS, Institut des Sciences Chimiques de Rennes, UMR 6226, F-35042 Rennes, France. E-mail: [sophie.guillaume@univ-rennes1.fr](mailto:sophie.guillaume@univ-rennes1.fr), [jean-francois.carpentier@univ-rennes1.fr](mailto:jean-francois.carpentier@univ-rennes1.fr)

<sup>b</sup> Univ. Libanaise, Campus Universitaire Rafic Hariri Hadath, Faculté des Sciences, Laboratoire de Chimie Médicinale et des Produits Naturels, Beirut, Lebanon.

E-mail: [Alikassem.alaaeddine@ul.edu.lb](mailto:Alikassem.alaaeddine@ul.edu.lb)

<sup>c</sup> Centre Régional de Mesures Physiques de l'Ouest-CRMPO, ScanMAT UMS 2001, Université de Rennes 1, France

† Electronic Supplementary Information (ESI) available: complementing NMR and MS spectra, DSC thermograms of the BPL<sup>FG</sup>s and PBPL<sup>FG</sup>s and kinetics of the polymerizations of BPL<sup>FG</sup>s. See DOI: 10.1039/x0xx00000x

‡ These authors performed all the experimental work (except the mass spectrometry (P.J.) and chiral HPLC (M.B.) analyses) and contributed to the writing of the paper.

## List of Tables, Schemes, and Figures

**Table S1.** Kinetic data for the monitoring of the ROP of *rac*-BPL<sup>CH2ZPh</sup>s with various 1/iPrOH (1:1) catalytic systems ([BPL<sup>CH2ZPh</sup>]<sub>0</sub>/[1]<sub>0</sub>/[iPrOH]<sub>0</sub> = 60:1:1; Figure 1).

**Table S2:** Tacticity and  $T_g$  values of PBPL<sup>FG</sup>s prepared by ROP of different functional BPL<sup>FG</sup>s with FG = CH<sub>2</sub>OPh, and CH<sub>2</sub>SPh, CH<sub>2</sub>CH<sub>2</sub>OCH<sub>2</sub>Ph, CH<sub>2</sub>OCH<sub>2</sub>Ph, using the catalytic systems **1a–1g**/iPrOH.

**Table S3:** Tacticity of PBPL<sup>FG</sup>s prepared by ROP of different (functional) BPL<sup>FG</sup>s with FG = Me, CH<sub>2</sub>OPh, CH<sub>2</sub>SPh, CH<sub>2</sub>CH<sub>2</sub>OCH<sub>2</sub>Ph, CH<sub>2</sub>OMe, CH<sub>2</sub>OAll, CH<sub>2</sub>OBn, and CO<sub>2</sub>All, CO<sub>2</sub>Bn, using the catalytic systems **1a–1g**/iPrOH.

**Figure S1.** Chiral HPLC chromatogram (column Chiralcel-OD DAICEL; 250 mm × 4.6 mm, 5 μm; 20 °C with a UV detector at 214 nm) of : (left) *racemic* phenyl glycidyl ether (*rac*-G<sup>CH2OPh</sup>), and (right) 99.97 % enantiopure phenyl glycidyl ether ((S)-G<sup>CH2OPh</sup>) (hexane/isopropanol 90/10; 1 mL·min<sup>-1</sup>, 22 bar).

**Figure S2.** <sup>1</sup>H NMR spectrum (400 MHz, CDCl<sub>3</sub>, 23 °C) of *racemic* 2-((phenylthio)methyl)oxirane (*rac*-G<sup>CH2SPh</sup>) (\*: residual water from the deuterated solvent).

**Figure S3.** Chiral HPLC chromatogram (column Chiralcel-OD DAICEL; 250 mm × 4.6 mm, 5 μm; 20 °C with a UV detector at 214 nm) of : (left) *racemic* 2-((phenylthio)methyl)oxirane (*rac*-G<sup>CH2SPh</sup>), and (right) 99.87% enantiopure (S)-2-((phenylthio)methyl)oxirane ((S)-G<sup>CH2SPh</sup>) (hexane/isopropanol 99.5/0.5; 0.9 mL·min<sup>-1</sup>, 23 bar).

**Figure S4.** <sup>1</sup>H NMR spectrum (400 MHz, CDCl<sub>3</sub>, 23 °C) of *racemic* 2-(2-(benzyloxy)ethyl)oxirane (*rac*-G<sup>CH2CH2OBn</sup>) (\*: residual water from the deuterated solvent).

**Figure S5.** Chiral HPLC chromatogram (column Chiralcel-OD DAICEL; 250 mm × 4.6 mm, 5 μm; 20 °C with a UV detector at 214 nm) of : (left) 2-(2-(benzyloxy)ethyl)oxirane (*rac*-G<sup>CH2CH2OBn</sup>), and (right) of 99.69% enantiopure (R)-2-(2-(benzyloxy)ethyl)oxirane ((R)-G<sup>CH2CH2OBn</sup>) (hexane/isopropanol 99.7/0.3; 1 mL·min<sup>-1</sup>, 25 bar).

**Figure S6.** <sup>1</sup>H NMR spectrum (500 MHz, CDCl<sub>3</sub>, 23 °C) (top) and <sup>13</sup>C (125 MHz, CDCl<sub>3</sub>, 25 °C) (bottom) of *racemic* 4-phenyloxymethylene-β-propiolactone (*rac*-BPL<sup>CH2OPh</sup>) (\*: residual water from the deuterated solvent).

**Figure S7.**  $^1\text{H}$  NMR spectrum (400 MHz,  $\text{CDCl}_3$ , 25 °C) (top) and  $^{13}\text{C}$  (100 MHz,  $\text{CDCl}_3$ , 25 °C) (bottom) of *racemic* 4-(phenylthio)methylene- $\beta$ -propiolactone (*rac*-BPL $^{\text{CH}_2\text{SPh}}$ ).

**Figure S8.** ESI-MS (ionized by  $\text{Na}^+$ , solvent  $\text{CH}_2\text{Cl}_2/\text{CH}_3\text{OH}$  (95/5 v:v)) of freshly synthesized *racemic* 4-(phenylthio)methylene- $\beta$ -propiolactone, *rac*-BPL $^{\text{CH}_2\text{SPh}}$  and ESI-MSMS of  $[\text{M}+\text{H}]^+$   $m/z$  195 with a collision energy of 10 eV. The zoomed region shows the peak for  $[(\text{COCH}_2\text{CH}(\text{CH}_2\text{SC}_6\text{H}_5)\text{O})\text{H}]\cdot\text{Na}^+$  ( $m/z$  = 217.0293). The two other fragmentation products depicted in red correspond to the loss of  $\text{CH}_2\text{CO}$  ( $m/z$  149), and to the subsequent loss of  $\text{CH}_2$  from the latter ( $m/z$  135), or to the loss of  $\text{CH}_2\text{CH}_2\text{CO}$  from the monomer, respectively.

**Figure S9.**  $^1\text{H}$  NMR spectrum (400 MHz,  $\text{CDCl}_3$ , 25 °C) showing the decomposed (**2**) and the rearrangement (**3**) products of *rac*-BPL $^{\text{CH}_2\text{SPh}}$ . Such rearrangements are known for  $\beta$ -lactones: J. W. Kramer, D. S. Treitler, G. W. Coates, Low Pressure Carbonylation of Epoxides to  $\beta$ -Lactones. *Organic Syntheses* **2003**, 86, 287-297.

**Figure S10.**  $^1\text{H}$  NMR spectrum (400 MHz,  $\text{CDCl}_3$ , 25 °C) (top) and  $^{13}\text{C}$  (100 MHz,  $\text{CDCl}_3$ , 25 °C) (bottom) of *racemic* 4-(2-(benzyloxy)ethylene)- $\beta$ -propiolactone, *rac*-BPL $^{\text{CH}_2\text{CH}_2\text{OCH}_2\text{Ph}}$ .

**Figure S11.** ESI-MS (ionized by  $\text{Na}^+$ , solvent  $\text{CH}_3\text{OH}$  of *racemic* 4-(2-(benzyloxy)ethylene)- $\beta$ -propiolactone, *rac*-BPL $^{\text{CH}_2\text{CH}_2\text{OCH}_2\text{Ph}}$ . Zoomed regions correspond to the experimental (middle) and simulated (bottom) spectra.

**Figure S12.**  $^1\text{H}$  NMR (500 MHz,  $\text{CDCl}_3$ , 25 °C) (top) and J-MOD (125 MHz,  $\text{CDCl}_3$ , 25 °C) (bottom) spectra of isotactic PBPL $^{\text{CH}_2\text{OPh}}$  prepared from the ROP of (*S*)-BPL $^{\text{CH}_2\text{OPh}}$  mediated by complex **1d** in the presence of *iPrOH* and precipitated twice in cold pentane (Table 1, entry 13).

**Figure S13.**  $^1\text{H}$  NMR (500 MHz,  $\text{CDCl}_3$ , 25 °C) (top) and J-MOD (125 MHz,  $\text{CDCl}_3$ , 25 °C) (bottom) spectra of isotactic PBPL $^{\text{CH}_2\text{SPh}}$  prepared from the ROP of (*S*)-BPL $^{\text{CH}_2\text{SPh}}$  mediated by complex **1d** in the presence of *iPrOH* and precipitated twice in cold pentane (Table 1, entry 27)

**Figure S14.**  $^1\text{H}$  (top) and  $^{13}\text{C}$  (bottom) NMR spectrum (500 and 125 MHz,  $\text{CDCl}_3$ , 25 °C) of isotactic PBPL $^{\text{CH}_2\text{CH}_2\text{OCH}_2\text{Ph}}$  prepared from the ROP of (*R*)-BPL $^{\text{CH}_2\text{CH}_2\text{OCH}_2\text{Ph}}$  mediated by complex **1d** in the presence of *iPrOH* and precipitated twice in cold pentane (Table 1, entry 40).

**Figure S15.**  $^1\text{H}$ - $^1\text{H}$  COSY NMR spectrum (500 MHz,  $\text{CDCl}_3$ , 25 °C) (top) and  $^1\text{H}$ - $^{13}\text{C}$  HMBC (500 MHz, 125 MHz,  $\text{CDCl}_3$ , 25 °C) (bottom) of syndiotactic PBPL $^{\text{CH}2\text{OPh}}$  precipitated twice in cold pentane (Table 1, entry 6) (\*: residual H-grease).

**Figure S16.**  $^1\text{H}$ - $^1\text{H}$  COSY NMR spectrum (500 MHz,  $\text{CDCl}_3$ , 25 °C) (top) and  $^1\text{H}$ - $^{13}\text{C}$  HMBC (500 MHz, 125 MHz,  $\text{CDCl}_3$ , 25 °C) (bottom) of syndiotactic PBPL $^{\text{CH}2\text{SPh}}$  precipitated twice in cold pentane (Table 1, entry 26).

**Figure S17.**  $^1\text{H}$ - $^1\text{H}$  COSY NMR spectrum (500 MHz,  $\text{CDCl}_3$ , 25 °C) (top) and  $^1\text{H}$ - $^{13}\text{C}$  HMBC (500 MHz, 125 MHz,  $\text{CDCl}_3$ , 25 °C) (bottom) of syndiotactic PBPL $^{\text{CH}2\text{CH}2\text{OCH}2\text{Ph}}$  precipitated twice in cold pentane (Table 1, entry 33).

**Figure S18.** (a) Details of  $^{13}\text{C}$  NMR spectrum (125 MHz,  $\text{CDCl}_3$ ) of *isotactic* PBPL $^{\text{CH}2\text{CH}2\text{OCH}2\text{Ph}}$ ; (b) a blend of *isotactic* PBPL $^{\text{CH}2\text{CH}2\text{OCH}2\text{Ph}}$  and PBPL $^{\text{CH}2\text{CH}2\text{OCH}2\text{Ph}}$  (Table 1, entries 40,39); (c) Details of  $^{13}\text{C}$  NMR spectrum of PBPL $^{\text{CH}2\text{CH}2\text{OCH}2\text{Ph}}$  (Table 1, entry 39).

**Figure S19.** MALDI-ToF MS (DCTB matrix, ionized by  $\text{Na}^+$ ) of PBPL $^{\text{CH}2\text{OPh}}$  precipitated twice in cold pentane (Table 1, entry 5). Right zoomed regions correspond to the simulated (top) and experimental (bottom) spectra.

**Figure S20.** ESI-MS (ionized by  $\text{Na}^+$ , solvent  $\text{CH}_3\text{OH}/\text{CH}_2\text{Cl}_2$  (90/10 v:v) of PBPL $^{\text{CH}2\text{SPh}}$  (Table 1, entry 24) precipitated twice in cold pentane; right zoom spectra are theoretical data (top) vs. experimental (bottom).

**Figure S21.** MALDI-ToF MS (DCTB matrix, ionized by  $\text{Na}^+$ ) of PBPL $^{\text{CH}2\text{CH}2\text{OCH}2\text{Ph}}$  precipitated twice in cold pentane (Table 1, entry 34). Zoomed regions correspond to the simulated (top) and experimental (bottom) spectra.

**Figure S22.** TGA thermograms of syndiotactic PBPL $^{\text{CH}2\text{OPh}}$  (top-left) (Table 1, entry 7); syndiotactic PBPL $^{\text{CH}2\text{SPh}}$  (top-right) (Table 1, entry 22); syndiotactic PBPL $^{\text{CH}2\text{CH}2\text{OCH}2\text{Ph}}$  (bottom-left) (Table 1, entry 38); and (bottom right) for PBPL $^{\text{Me}}$  ( $M_{n,\text{NMR}} = 7900 \text{ g mol}^{-1}$ ,  $D_M = 1.04$ ;  $P_r = 0.84$ ) prepared by ROP as previously reported (A. Amgoune, C. M. Thomas, S. Ilinca, T. Roisnel and J.-F. Carpentier, *Angew. Chem. Int. Ed.* 2006, **45**, 2782–2784).

**Figure S23.** DSC thermogram (heating rate of  $10 \text{ }^\circ\text{Cmin}^{-1}$ , second heating cycle, from  $-80$  to  $200 \text{ }^\circ\text{C}$ ) of: (left) syndiotactic PBPL $^{\text{CH}2\text{OPh}}$  ( $P_r 0.75$ ) synthesized by ROP of *rac*-BPL $^{\text{CH}2\text{OPh}}$  with Y{ONNO $^{\text{Cl}2}$ }/(*i*PrOH) (Table 1, entry 4); (right) syndiotactic PBPL $^{\text{CH}2\text{OPh}}$  ( $P_r 0.83$ ) synthesized by ROP of *rac*-BPL $^{\text{CH}2\text{OPh}}$  with Y{ONNO $^{\text{tBu}2}$ }/(*i*PrOH) (Table 1, entry 12).

**Figure S24.** DSC thermogram (heating rate of  $10\text{ }^{\circ}\text{C min}^{-1}$ , second heating cycle  $-80$  to  $200\text{ }^{\circ}\text{C}$ ) of: (left) syndiotactic  $\text{PBPL}^{\text{CH2SPh}} (P_r 0.76)$  synthesized by ROP of *rac*- $\text{BPL}^{\text{CH2SPh}}$  with  $\text{Y}\{\text{ONNO}^{\text{Me}2}\}/(i\text{PrOH})$  (Table 1, entry 15); (right) syndiotactic  $\text{PBPL}^{\text{CH2SPh}} (P_r 0.86)$  synthesized by ROP of *rac*- $\text{BPL}^{\text{CH2SPh}}$  with  $\text{Y}\{\text{ONNO}^{\text{tBu}2}\}/(i\text{PrOH})$  (Table 1, entry 21).

**Figure S25.** DSC thermogram (heating rate of  $10\text{ }^{\circ}\text{Cmin}^{-1}$ , second heating cycle  $-60$  to  $200\text{ }^{\circ}\text{C}$ ) of : (left) syndiotactic  $\text{PBPL}^{\text{CH2CH2OCH2Ph}} (P_r 0.86)$  synthesized by ROP of *rac*- $\text{BPL}^{\text{CH2CH2OCH2Ph}}$  with  $\text{Y}\{\text{ONNO}^{\text{cumyl}2}\}/(i\text{PrOH})$  (Table 1, entry 36); (right) atactic  $\text{PBPL}^{\text{CH2CH2OCH2Ph}} (P_r 0.49)$  synthesized by ROP of *rac*- $\text{BPL}^{\text{CH2CH2OCH2Ph}}$  with  $\text{Y}\{\text{ONNO}^{\text{Cl}2}\}/(i\text{PrOH})$  (Table 1, entry 31).

**Table S1.** Kinetic data for the monitoring of the ROP of *rac*-BPL<sup>CH2ZPh</sup>s with various **1**/iPrOH (1:1) catalytic systems ([BPL<sup>CH2ZPh</sup>]<sub>0</sub>/[**1**]<sub>0</sub>/[iPrOH]<sub>0</sub> = 60:1:1; Figure 1).

BPL <sup>CH2ZPh</sup> Catalyst <b>1</b>	Time (h)	Conv. (%)	ln([BPL <sup>CH2ZPh</sup> ] <sub>0</sub> /[BPL <sup>CH2ZPh</sup> ] <sub>t</sub> )	M <sub>n, theo</sub> (g.mol <sup>-1</sup> )	M <sub>n,NMR</sub> (g.mol <sup>-1</sup> )	M <sub>n,SEC</sub> (g.mol <sup>-1</sup> )	D <sub>M</sub>
<b>Table 1, entry 4</b>	0	0	0	0	0	0	-
BPL <sup>CH2OPh</sup>	1.17	19	0.21	3 000	2 500	3 500	1.09
{ONNO} <sup>Cl2</sup>	4	38	0.48	4 100	3 900	4 300	1.10
<b>1c</b>	7	48	0.65	5 100	5 000	5 200	1.13
	50	54	-	5 800	5 400	6 200	1.15
<b>Table 1, entry 2</b>	0	0	0	0	0	0	-
BPL <sup>CH2OPh</sup>	0.25	20	0.22	2 200	2 000	2 600	1.11
{ONNO} <sup>Me2</sup>	0.50	40	0.51	4 300	5 700	5 100	1.11
<b>1a</b>	1.17	64	1.03	6 900	6 900	8 200	1.13
	2.17	83	1.78	8 900	8 000	10 400	1.13
	4.17	95	3.22	10 200	10 000	11 100	1.13
<b>Table 1, entry 11</b>	0	0	0	0	0	0	-
BPL <sup>CH2OPh</sup>	0.14	100	4.61	10 700	10 000	12 200	1.12
{ONNO} <sup>Cumyl2</sup>	0.5	100	-	10 700	10 000	12 200	1.15
<b>Table 1, entry 6</b>	0	0	0	0	0	0	-
BPL <sup>CH2OPh</sup>	0.14	100	4.61	10 700	10 600	12 200	1.11
{ONNO} <sup>tBu2</sup>	0.25	100	-	10 700	10 600	12 200	1.14
<b>Table 1, entry 18</b>	0	0	0	0	0	0	-
BPL <sup>CH2SPh</sup>	24	12	0.13	1 500	1 300	1 600	1.08
{ONNO} <sup>Cl2</sup>	48	21	0.24	2 500	2 400	2 600	1.12
<b>1c</b>	60	28	0.33	3 300	3 200	3 600	1.14
	96	48	-	5 700	5 100	6 400	1.17
<b>Table 1, entry 15</b>	0	0	0	0	0	0	-
BPL <sup>CH2SPh</sup>	0.25	10	0.11	1 200	1 100	1 500	1.13
{ONNO} <sup>Me2</sup>	0.5	20	0.22	2 400	2 400	3 200	1.14
<b>1a</b>	2	55	0.80	6 400	6 300	8 900	1.16
	4	88	2.12	10 400	10 200	12 500	1.18
	8	99	4.61	11 600	11 300	13 900	1.21
<b>Table 1, entry 25</b>	0	0	0	0	0	0	-
BPL <sup>CH2SPh</sup>	0.17	100	4.61	11 700	11 300	12 700	1.08
{ONNO} <sup>Cumyl2</sup>	1	100	-	11 700	11 300	13 300	1.12
<b>Table 1, entry 20</b>	0	0	0	0	0	0	-
BPL <sup>CH2SPh</sup>	0.17	100	4.61	15 600	15 200	16 200	1.07
{ONNO} <sup>tBu2</sup>	1	100	4.61	15 600	15 200	17 900	1.15

<b>BPL<sup>CH2ZPh</sup></b> <b>Catalyst 1</b>	<b>Time (h)</b>	<b>Conv. (%)</b>	<b>ln([BPL<sup>CH2ZPh</sup>]<sub>0</sub>/[BPL<sup>CH2ZPh</sup>]<sub>t</sub>)</b>	<b>M<sub>n, theo</sub> (g.mol<sup>-1</sup>)</b>	<b>M<sub>n,NMR</sub> (g.mol<sup>-1</sup>)</b>	<b>M<sub>n,SEC</sub> (g.mol<sup>-1</sup>)</b>	<b>D<sub>M</sub></b>
<i>1</i> <b>BPL<sup>CH2CH2OBn</sup></b> <b>{ONNO}<sup>Me2</sup></b> <b>1a</b>	1	11	0.118	1400	1300	1400	1.05
	2	19	0.213	2400	2200	2000	1.07
	3	27	0.311	3300	3200	2700	1.07
	4	31	0.375	3900	3400	3100	1.07
	9	46	0.625	5800	5500	4300	1.07
<i>2</i> <b>BPL<sup>CH2CH2OBn</sup></b> <b>{ONNO}<sup>Cl2</sup></b> <b>1c</b>	1	8	0.081	1000	1100	1300	1.08
	2	13	0.143	1700	1600	2100	1.08
	3	19	0.211	2400	2500	2600	1.09
	4	21	0.234	2600	2700	2800	1.09
	9	33	0.402	4100	3900	3700	1.13
<i>3</i> <b>BPL<sup>CH2CH2OBn</sup></b> <b>{ONNO}<sup>tBu2</sup></b> <b>1d</b>	0.5min	35	0.439	4400	4000	3600	1.08
	1 min	66	1.07	8200	7600	6600	1.09
	2 min	90	2.31	11200	11000	8700	1.07
	3 min	96	3.27	11900	11200	9400	1.07
	5 min	100	-	12400	11900	9400	1.08
<i>4</i> <b>BPL<sup>CH2CH2OBn</sup></b> <b>{ONNO}<sup>Cumyl2</sup></b> <b>1f</b>	0.5min	8	0.088	1100	1000	1600	1.07
	1 min	17	0.19	2200	2000	2300	1.09
	2 min	35	0.428	4300	4100	3800	1.09
	3 min	50	0.687	6200	5600	4900	1.08
	4 min	61	0.952	7600	7200	6200	1.08
	5 min	71	1.25	8900	8100	7200	1.08

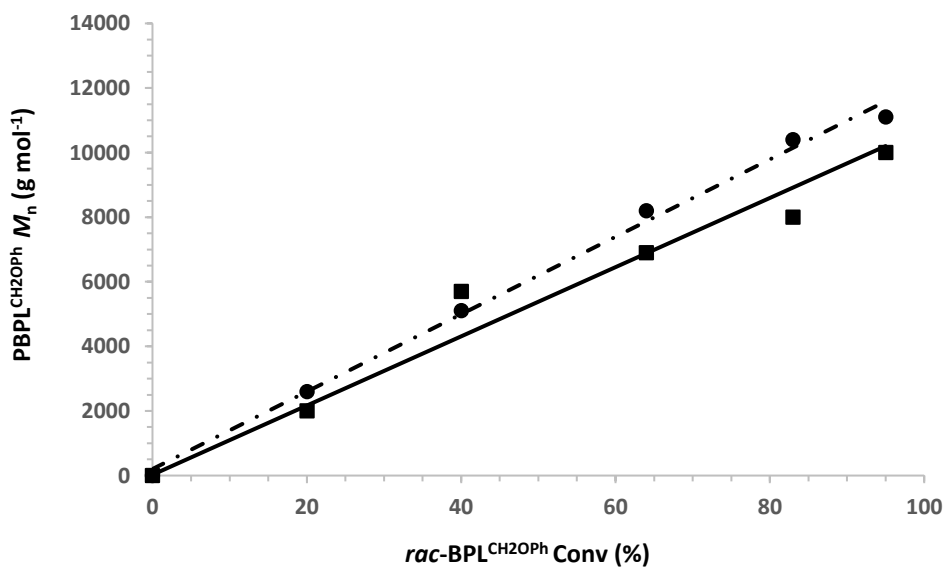


**Table 1 Entry 2:** Variation of M<sub>n,NMR</sub> ■, M<sub>n,SEC</sub> ●, and M<sub>n, theo</sub> (solid line) values of PBPL<sup>CH2OPh</sup>s synthesized from the ROP of rac-BPL<sup>CH2OPh</sup>s mediated by **1a**/(iPrOH) (1:1) catalytic system as a function of the monomer conversion.

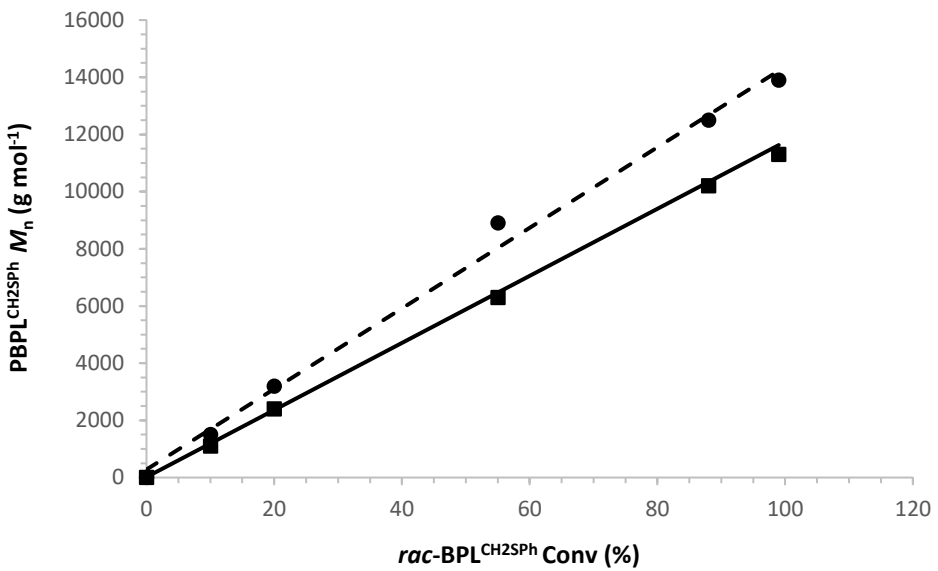


**Table 1 Entry 15:** Variation of  $M_{n,NMR}$  ■,  $M_{n,SEC}$  ●, and  $M_{n,\text{theo}}$  (solid line) values of  $\text{PBPL}^{\text{CH}_2\text{SPH}}$ s synthesized from the ROP of *rac*-BPL<sup>CH<sub>2</sub>SPH</sup>s mediated by **1a**/(iPrOH) (1:1) catalytic system as a function of the monomer conversion .

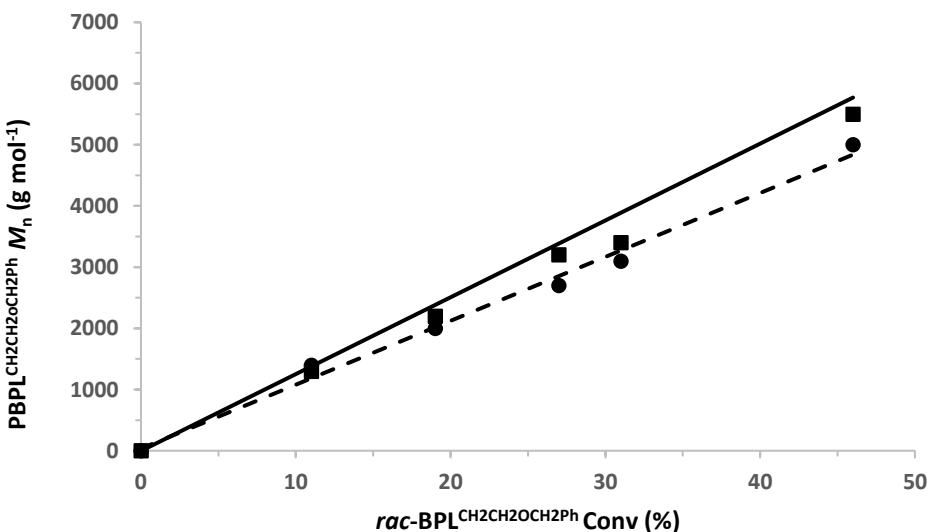


**Table S1 Entry 1:** Variation of  $M_{n,NMR}$  ■,  $M_{n,SEC}$  ●, and  $M_{n,\text{theo}}$  (solid line) values of  $\text{PBPL}^{\text{CH}_2\text{CH}_2\text{OCH}_2\text{Ph}}$ s synthesized from the ROP of *rac*-BPL<sup>CH<sub>2</sub>CH<sub>2</sub>OCH<sub>2</sub>Ph</sup>s mediated by **1a**/(iPrOH) (1:1) catalytic system as a function of the monomer conversion.

**Table S2:** Tacticity and  $T_g$  values of PBPL<sup>FG</sup>s prepared by ROP of different functional BPL<sup>FG</sup>s with FG = CH<sub>2</sub>OPh, and CH<sub>2</sub>SPh, CH<sub>2</sub>CH<sub>2</sub>OCH<sub>2</sub>Ph, CH<sub>2</sub>OCH<sub>2</sub>Ph, using the catalytic systems **1a–1g/iPrOH**.

Cat.\BPL <sup>FG</sup>	BPL <sup>CH2OPh</sup>	BPL <sup>CH2SPh</sup>	BPL <sup>CH2CH2OCH2Ph</sup>	BPL <sup>CH2OCH2Ph</sup>
<b>1a,b</b>	Syndiotactic $P_r = 0.76\text{--}0.79$ $T_g = 30\text{ }^\circ\text{C}$	Syndiotactic $P_r = 0.74\text{--}0.76$ $T_g = 8, 9\text{ }^\circ\text{C}$	Atactic $P_r = 0.49\text{--}0.52$ $T_g = -11\text{ }^\circ\text{C}$	Atactic * $P_r = 0.50$ $T_g = -6\text{ }^\circ\text{C}$
<b>1c</b>	Syndiotactic $P_r = 0.75\text{--}0.77$ $T_g = 21, 22\text{ }^\circ\text{C}$	Syndiotactic $P_r = 0.73\text{--}0.74$ $T_g = 9\text{ }^\circ\text{C}$	Atactic $P_r = 0.49$ $T_g = -13\text{ }^\circ\text{C}$	Isotactic * $P_r = 0.10$ $T_g = -1\text{ }^\circ\text{C}$
<b>1d–1g</b>	Syndiotactic $P_r = 0.81\text{--}0.87$ $T_g = 36\text{--}40\text{ }^\circ\text{C}$	Syndiotactic $P_r = 0.83\text{--}0.87$ $T_g = 12\text{--}14\text{ }^\circ\text{C}$	Syndiotactic $P_r = 0.77\text{--}0.86$ $T_g = -8\text{--}13\text{ }^\circ\text{C}$	Syndiotactic * $P_r = 0.85\text{--}0.90$ $T_g = 0\text{ }^\circ\text{C}$

\* (a) Ligny, R.; Hanninen, M. M.; Guillaume, S. M.; Carpentier, J. F. *Angew. Chem. Int. Ed.* **2017**, *56* (35), 10388–10393; (b) Ligny, R.; Hänninen, M. M.; Guillaume, S. M.; Carpentier, J.-F., *Chem. Commun.* **2018**, *54* (58), 8024–8031.

**Table S3:** Tacticity of PBPL<sup>FG</sup>s prepared by ROP of different (functional) BPL<sup>FG</sup>s with FG = Me, CH<sub>2</sub>OPh, CH<sub>2</sub>SPh, CH<sub>2</sub>CH<sub>2</sub>OCH<sub>2</sub>Ph, CH<sub>2</sub>OMe, CH<sub>2</sub>OAll, CH<sub>2</sub>OBn, and CO<sub>2</sub>All, CO<sub>2</sub>Bn, using the catalytic systems **1a–1g** /iPrOH.

BPL <sup>FG</sup> Cat.	BPL <sup>Me</sup>	BPL <sup>CH<sub>2</sub>OPh/SPh</sup>	BPL <sup>CH<sub>2</sub>OMe/All/Bn</sup>	BPL <sup>CH<sub>2</sub>CH<sub>2</sub>OCH<sub>2</sub>Ph</sup>	BPL <sup>CO<sub>2</sub>All/Bn</sup>
Crowded	Syndiotactic ‡ $P_r = 0.70\text{--}0.96$	Syndiotactic $P_r = 0.81\text{--}0.87$	Syndiotactic * $P_r = 0.78\text{--}0.90$	Syndiotactic $P_r = 0.77\text{--}0.86$	Syndiotactic † $P_r = 0.68\text{--}0.87$
Non-crowded	Atactic ‡ $P_r = 0.56$	Syndiotactic $P_r = 0.74\text{--}0.79$	Atactic * $P_r = 0.49\text{--}0.51$	Atactic $P_r = 0.49\text{--}0.52$	Syndiotactic † $P_r = 0.92\text{--}>0.95$
Halogenated non-crowded	Atactic ‡ $P_r = 0.42\text{--}0.45$	Syndiotactic $P_r = 0.73\text{--}0.77$	Isotactic * $P_r = <0.05\text{--}0.12$	Atactic $P_r = 0.49$	Syndiotactic † $P_r = 0.91\text{--}>0.98$

‡ (a) Chapurina, Y.; Klitzke, J.; Casagrande Ode, L., Jr.; Awada, M.; Dorcet, V.; Kirillov, E.; Carpentier, J. F. *Dalton Trans* **2014**, 43 (38), 14322–14333; (b) Bouyahyi, M.; Ajellal, N.; Kirillov, E.; Thomas, C. M.; Carpentier, J.-F. *Chem. –Eur. J.*, **2011**, 17, 1872–1883; (c) Amgoune, A.; Thomas, C. M.; Ilinca, S.; Roisnel, T.; Carpentier, J.-F. *Angew. Chem. Int. Ed.* **2006**, 118 (17), 2848–2850.

\* (a) Ligny, R.; Hanninen, M. M.; Guillaume, S. M.; Carpentier, J. F. *Angew. Chem. Int. Ed.* **2017**, 56 (35), 10388–10393; (b) Ligny, R.; Hänninen, M. M.; Guillaume, S. M.; Carpentier, J.-F. *Chem. Commun.* **2018**, 54 (58), 8024–8031; (c) Ligny, R.; Guillaume, S. M.; Carpentier, J. F., *Chem. –Eur. J.*, **2019**, 25, 6412–6424.

† (a) Jaffredo, C. G.; Chapurina, Y.; Kirillov, E.; Carpentier, J. F.; Guillaume, S. M. *Chem. –Eur. J.*, **2016**, 22 (22), 7629–7641; (b) Jaffredo, C. G.; Chapurina, Y.; Guillaume, S. M.; Carpentier, J. F. *Angew Chem. Int. Ed.* **2014**, 53 (10), 2687–2691.

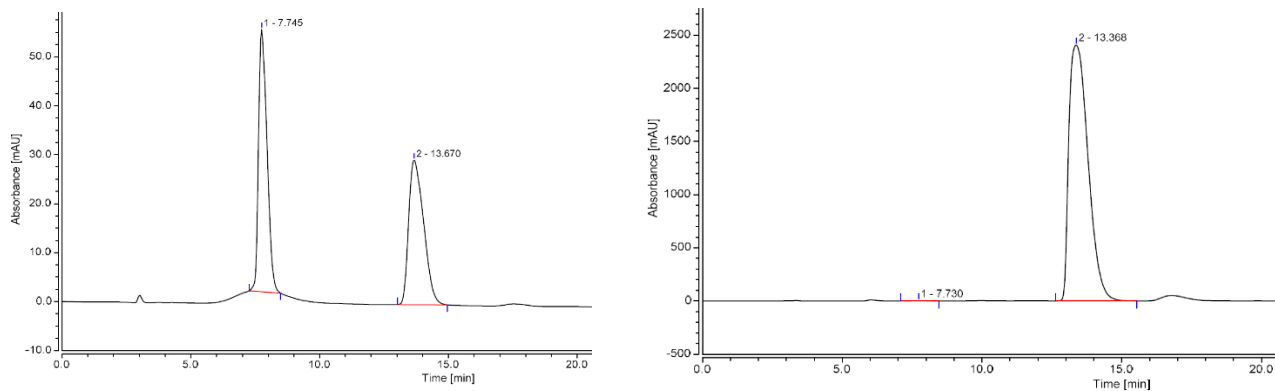


**Figure S1.** Chiral HPLC chromatogram (column Chiralcel-OD DAICEL; 250 mm × 4.6 mm, 5 $\mu$ m; 20 °C with a UV detector at 214 nm) of : (left) *racemic* phenyl glycidyl ether (*rac*-G<sup>CH<sub>2</sub>OPh</sup>), and (right) 99.97 % enantiopure phenyl glycidyl ether ((*S*)-G<sup>CH<sub>2</sub>OPh</sup>) (hexane/isopropanol 90/10; 1 mL·min<sup>-1</sup>, 22 bar).

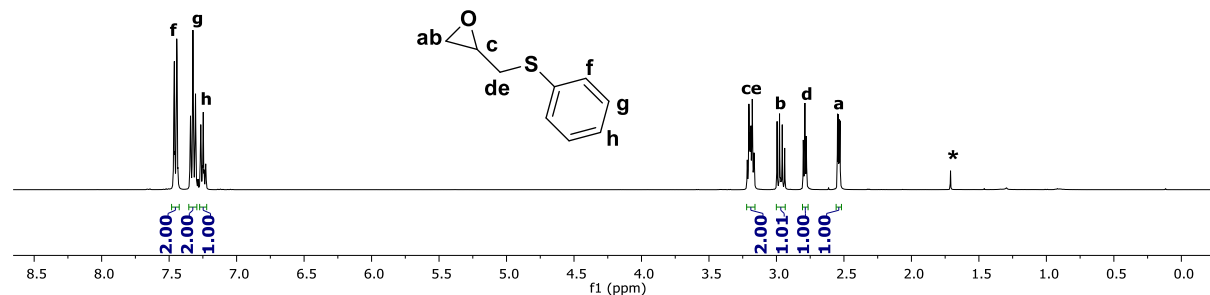


**Figure S2.** <sup>1</sup>H NMR spectrum (400 MHz, CDCl<sub>3</sub>, 23 °C) of *racemic* 2-((phenylthio)methyl)oxirane (*rac*-G<sup>CH<sub>2</sub>SPh</sup>) (\*: residual water from the deuterated solvent).

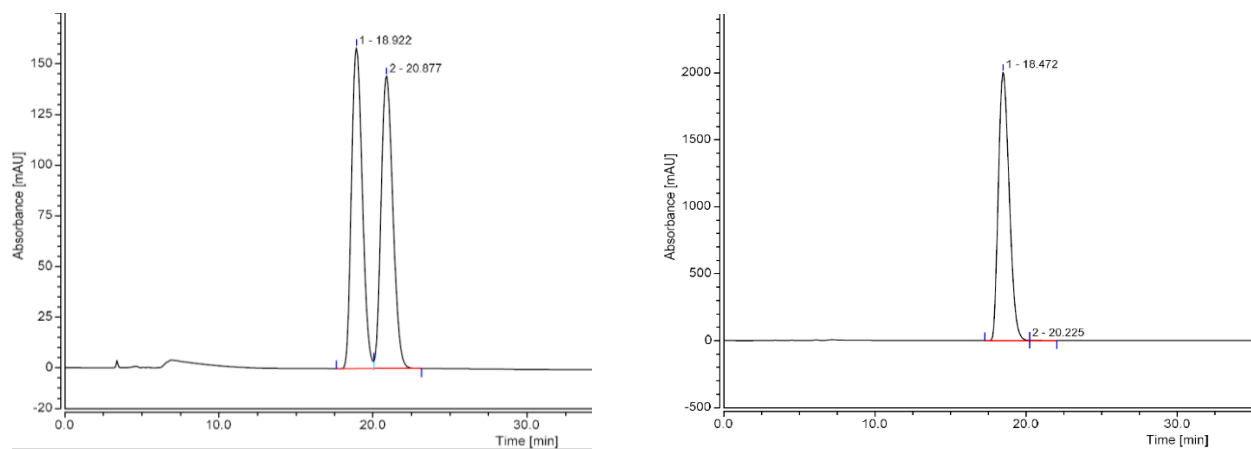


**Figure S3.** Chiral HPLC chromatogram (column Chiralcel-OD DAICEL; 250 mm × 4.6 mm, 5 µm; 20 °C with a UV detector at 214 nm) of : (left) *racemic* 2-((phenylthio)methyl)oxirane (*rac*-G<sup>CH2SPh</sup>), and (right) 99.87% enantiopure (*S*)-2-((phenylthio)methyl)oxirane ((*S*)-G<sup>CH2SPh</sup>) (hexane/isopropanol 99.5/0.5; 0.9 mL·min<sup>-1</sup>, 23 bar).

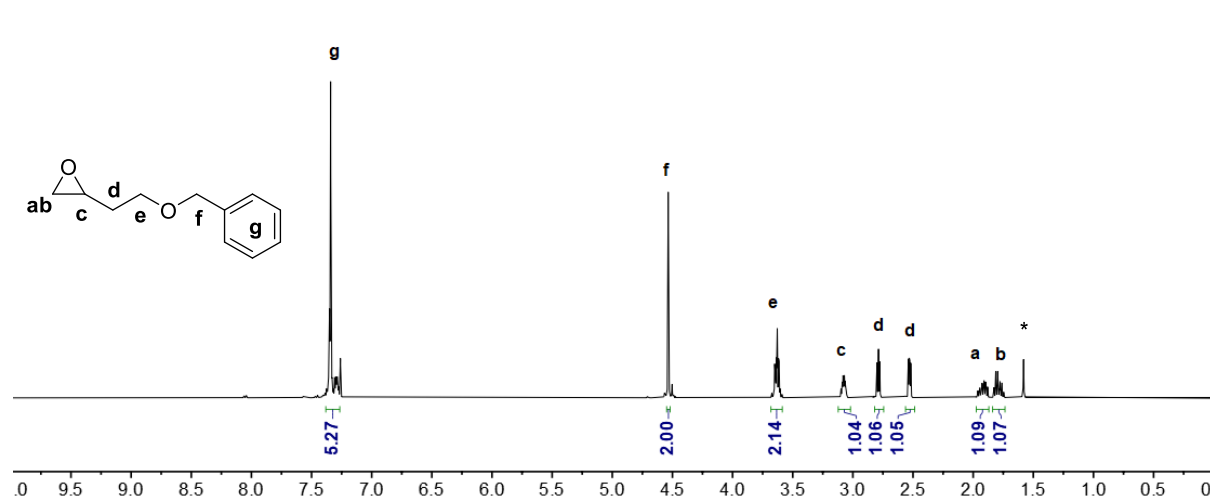


**Figure S4.** <sup>1</sup>H NMR spectrum (400 MHz, CDCl<sub>3</sub>, 23 °C) of *racemic* 2-(2-(benzyloxy)ethyl)oxirane (*rac*-G<sup>CH2CH2OBn</sup>) (\*: residual water from the deuterated solvent).

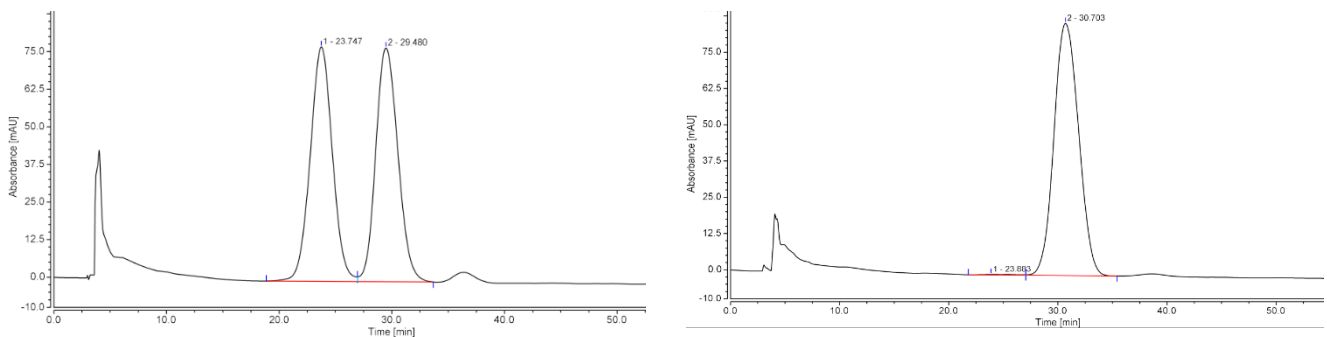


**Figure S5.** Chiral HPLC chromatogram (column Chiralcel-OD DAICEL; 250 mm × 4.6 mm, 5 µm; 20 °C with a UV detector at 214 nm) of : (left) 2-(2-(benzyloxy)ethyl)oxirane (*rac*-G<sup>CH2CH2OBn</sup>), and (right) of 99.69% enantiopure (*R*)-2-(2-(benzyloxy)ethyl)oxirane ((*R*)-G<sup>CH2CH2OBn</sup>) (hexane/isopropanol 99.7/0.3; 1 mL·min<sup>-1</sup>, 25 bar) .

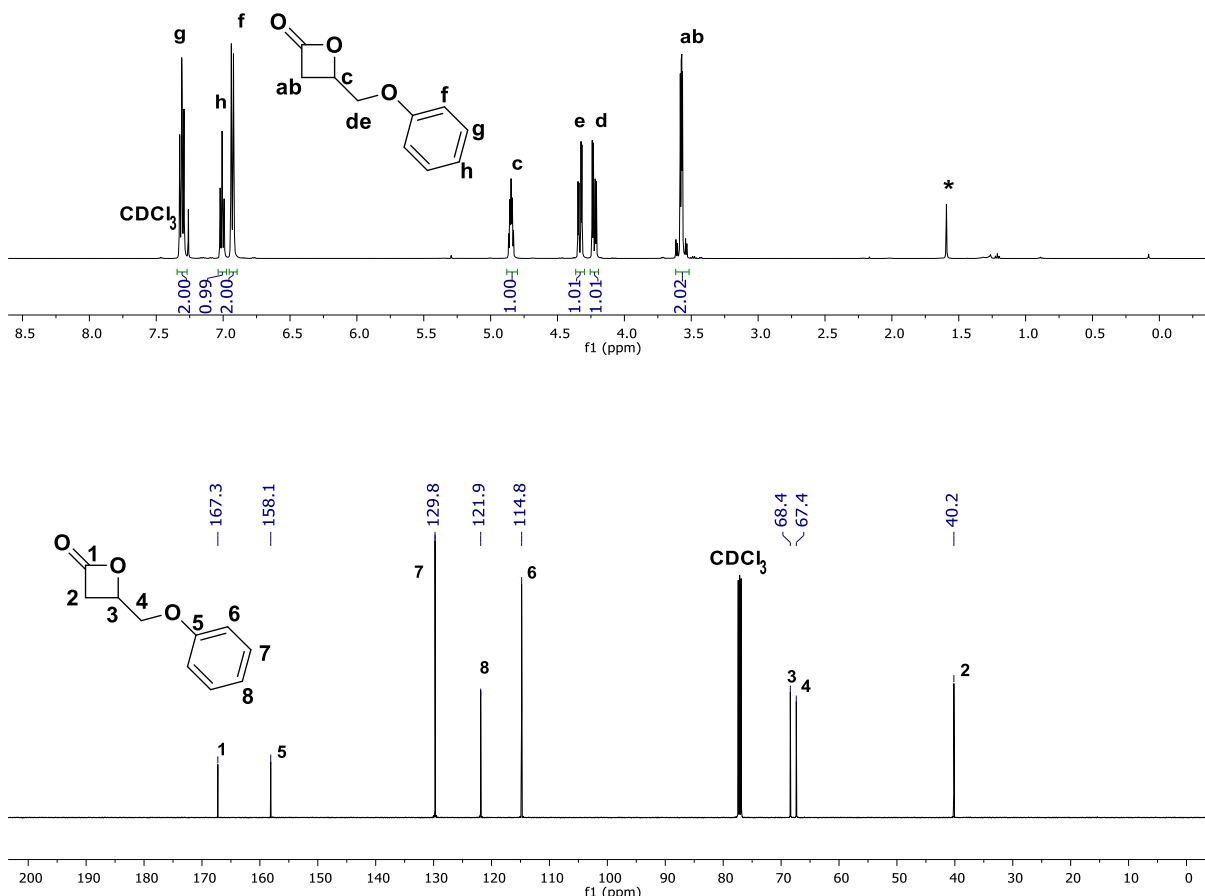


**Figure S6.** <sup>1</sup>H NMR spectrum (500 MHz, CDCl<sub>3</sub>, 23 °C) (top) and <sup>13</sup>C (125 MHz, CDCl<sub>3</sub>, 25 °C) (bottom) of *racemic* 4-phenyloxymethylene-β-propiolactone (*rac*-BPL<sup>CH2OPh</sup>) (\*: residual water from the deuterated solvent).

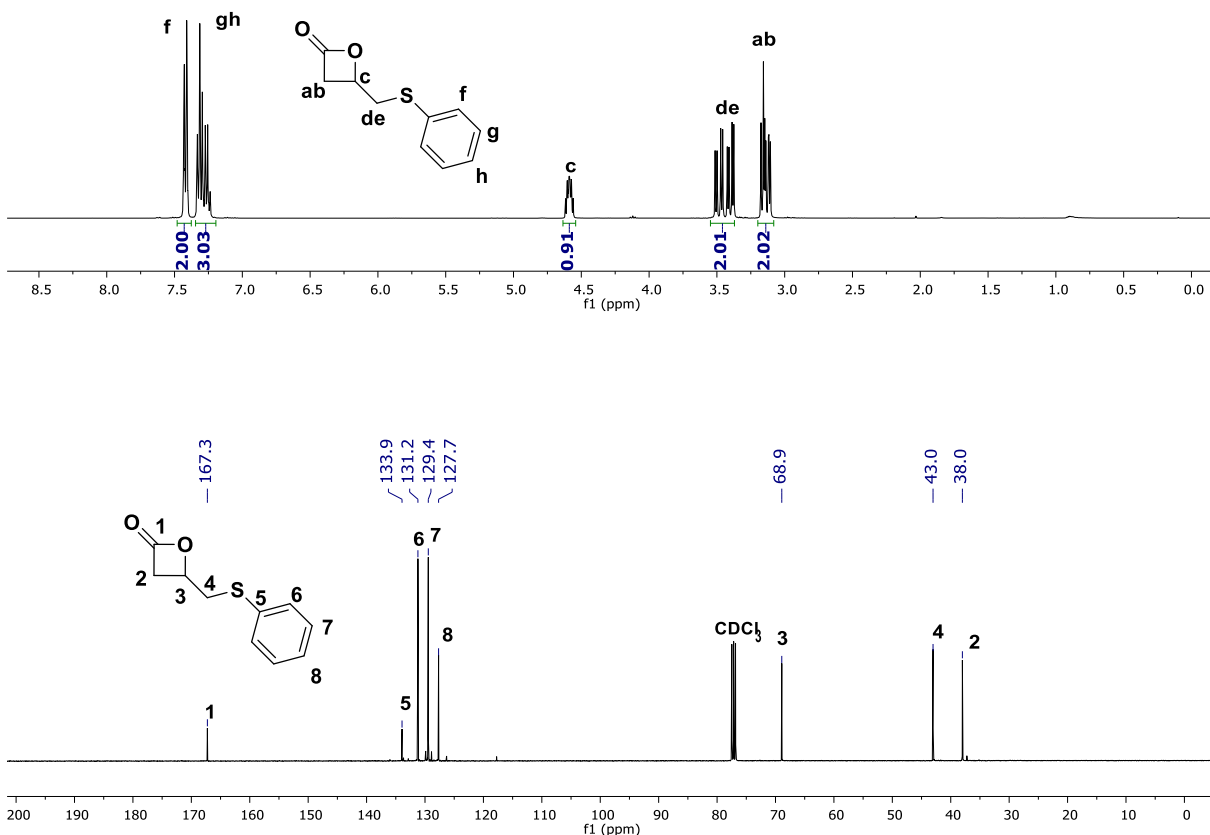


**Figure S7.**  $^1\text{H}$  NMR spectrum (400 MHz, CDCl<sub>3</sub>, 25 °C) (top) and  $^{13}\text{C}$  (100 MHz, CDCl<sub>3</sub>, 25 °C) (bottom) of *racemic* 4-(phenylthio)methylene- $\beta$ -propiolactone (*rac*-BPL<sup>CH<sub>2</sub>SPh</sup>).

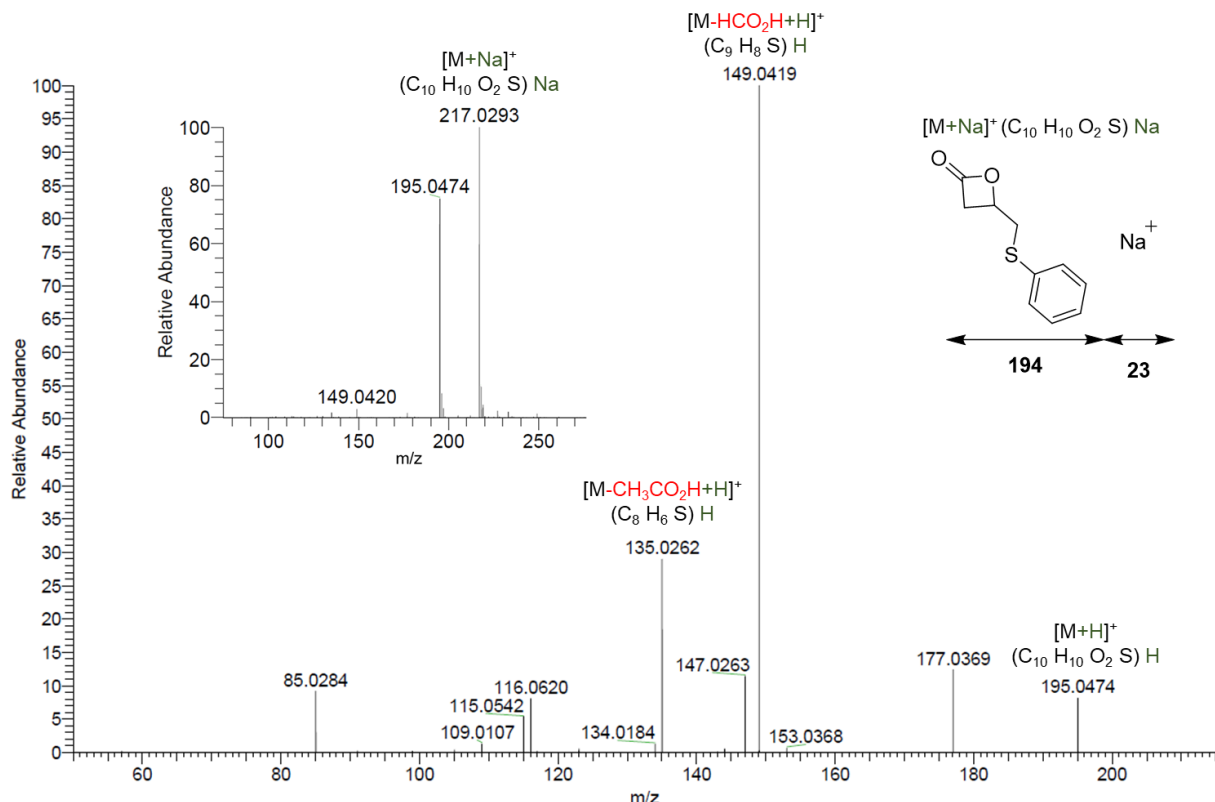
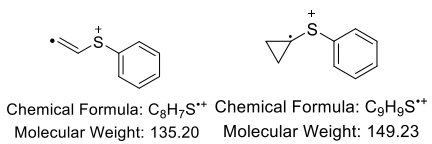


**Figure S8.** ESI-MS (ionized by  $\text{Na}^+$ , solvent  $\text{CH}_2\text{Cl}_2/\text{CH}_3\text{OH}$  (95/5 v:v)) of freshly synthesized *racemic* 4-(phenylthio)methylene- $\beta$ -propiolactone, *rac*-BPL <sup>$\text{CH}_2\text{SPh}$</sup>  and ESI-MSMS of  $[\text{M}+\text{H}]^+$   $m/z$  195 with a collision energy of 10 eV. The zoomed region shows the peak for  $[(\text{COCH}_2\text{CH}(\text{CH}_2\text{SC}_6\text{H}_5)\text{O})\text{H}]\cdot\text{Na}^+$  ( $m/z$  = 217.0293). The two other fragmentation products depicted in red correspond to the loss of  $\text{CH}_2\text{CO}$  ( $m/z$  149), and to the subsequent loss of  $\text{CH}_2$  from the latter ( $m/z$  135), or to the loss of  $\text{CH}_2\text{CH}_2\text{CO}$  from the monomer, respectively.

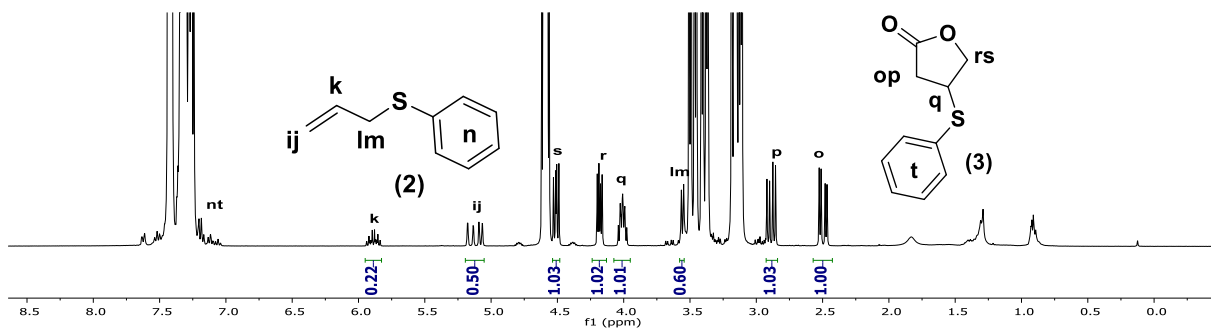


**Figure S9.** <sup>1</sup>H NMR spectrum (400 MHz, CDCl<sub>3</sub>, 25 °C) showing the decomposed (**2**) and the rearrangement (**3**) products of *rac*-BPL<sup>CH2SPh</sup>. Such rearrangements are known for β-lactones: J. W. Kramer, D. S. Treitler, G. W. Coates, Low Pressure Carbonylation of Epoxides to β-Lactones. *Organic Syntheses* **2003**, 86, 287-297.

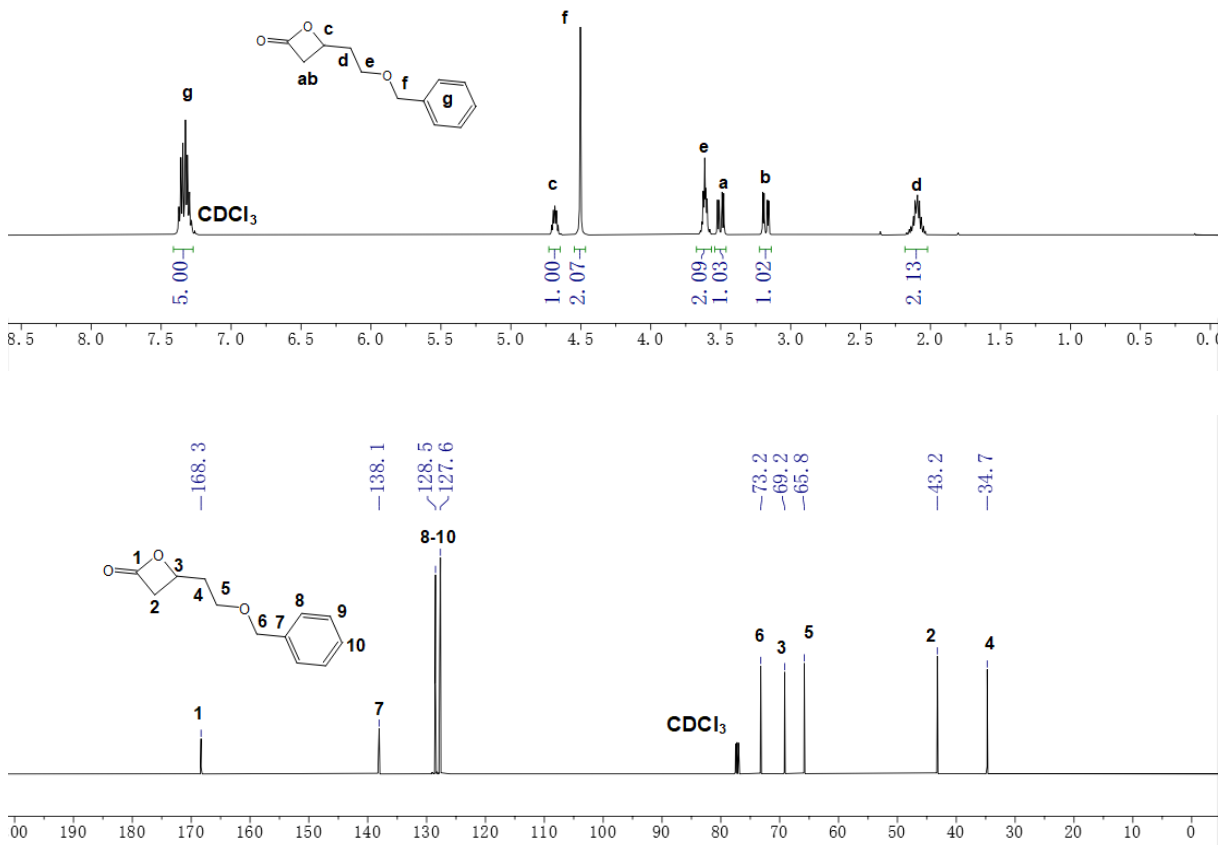


**Figure S10.** <sup>1</sup>H NMR spectrum (400 MHz, CDCl<sub>3</sub>, 25 °C) (top) and <sup>13</sup>C (100 MHz, CDCl<sub>3</sub>, 25 °C) (bottom) of *racemic* 4-(2-(benzyloxy)ethylene)-β-propiolactone, *rac*-BPL<sup>CH2CH2OCH2Ph</sup>.

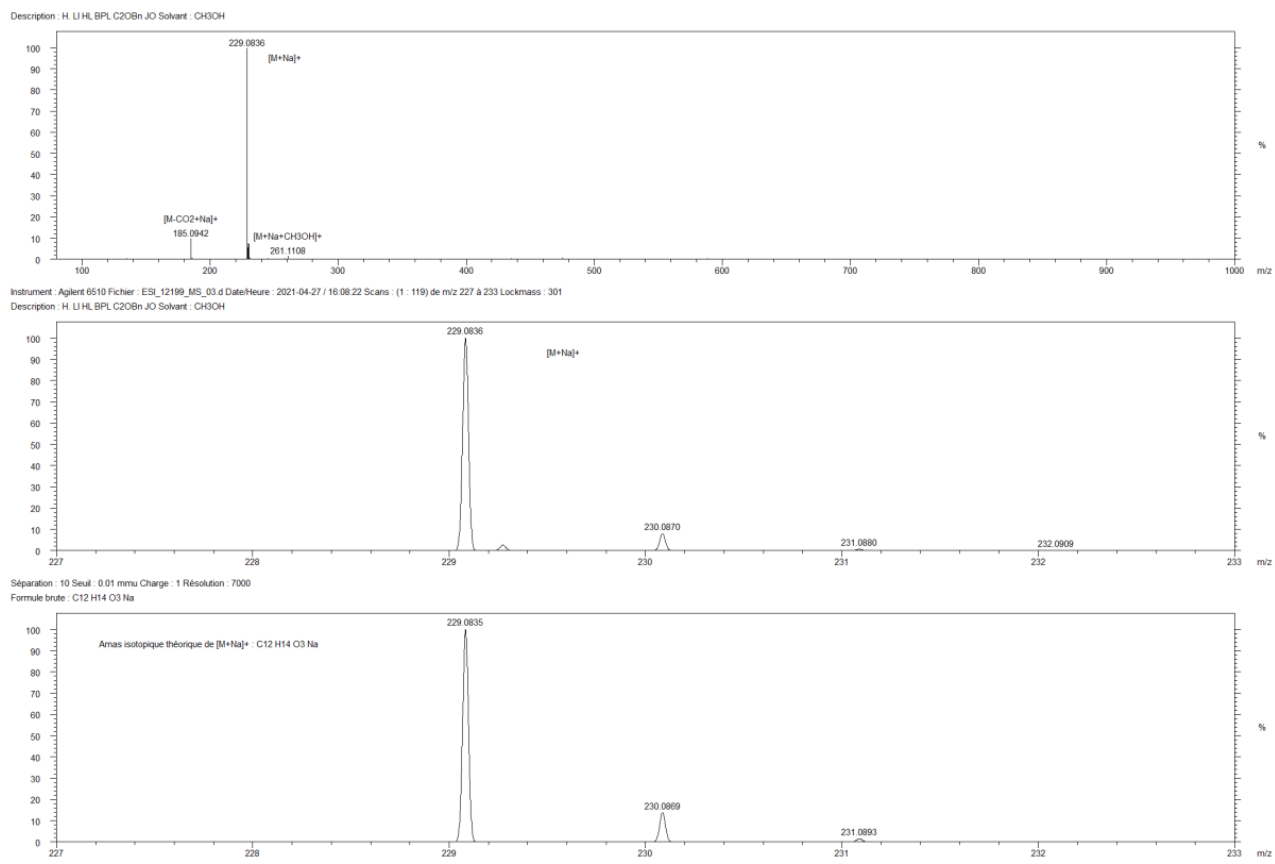


**Figure S11.** ESI-MS (ionized by Na<sup>+</sup>, solvent CH<sub>3</sub>OH of *racemic* 4-(2-(benzyloxy)ethylene)- $\beta$ -propiolactone, *rac*-BPL<sup>CH<sub>2</sub>CH<sub>2</sub>OCH<sub>2</sub>Ph</sup>. Zoomed regions correspond to the experimental (middle) and simulated (bottom) spectra.

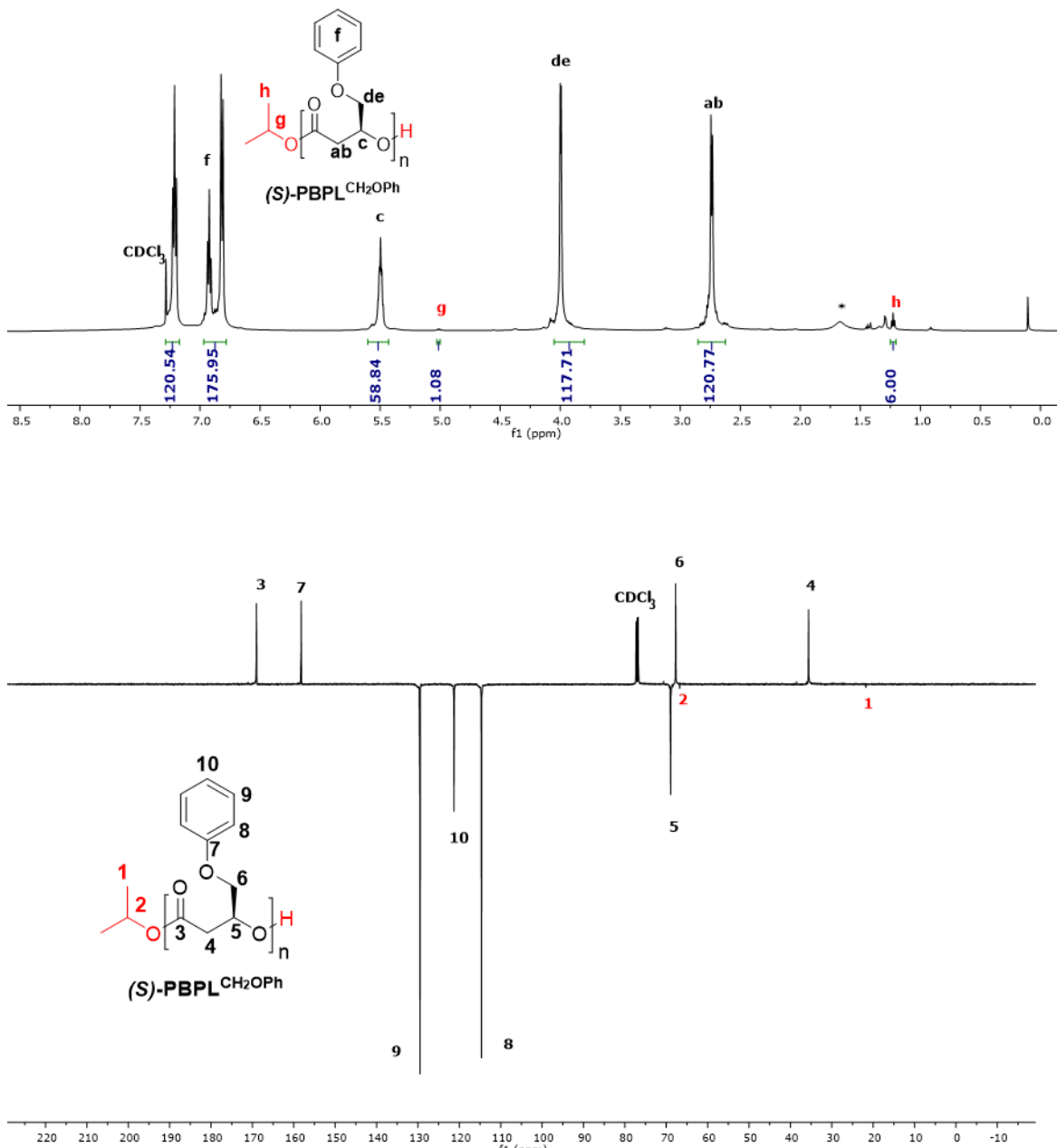


**Figure S12.** <sup>1</sup>H NMR (500 MHz, CDCl<sub>3</sub>, 25 °C) (top) and J-MOD (125 MHz, CDCl<sub>3</sub>, 25 °C) (bottom) spectra of isotactic PBPL<sup>CH<sub>2</sub>OPh</sup> prepared from the ROP of (S)-BPL<sup>CH<sub>2</sub>OPh</sup> mediated by complex **1d** in the presence of *i*PrOH and precipitated twice in cold pentane (Table 1, entry 13), \* residual water.

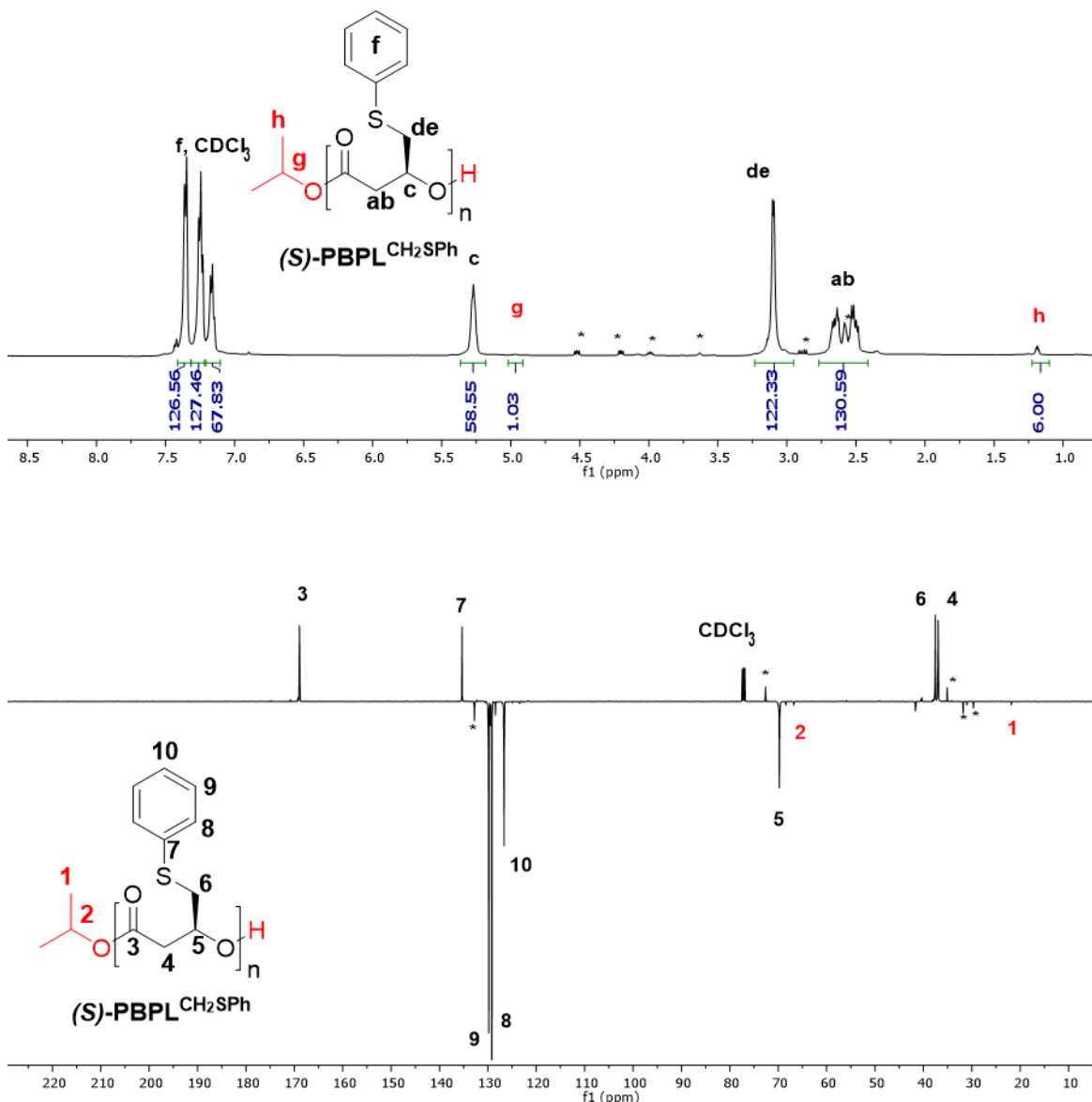


**Figure S13.** <sup>1</sup>H NMR (500 MHz, CDCl<sub>3</sub>, 25 °C) (top) and J-MOD (125 MHz, CDCl<sub>3</sub>, 25 °C) (bottom) spectra of isotactic PBPL<sup>CH<sub>2</sub>SPh</sup> prepared from the ROP of (S)-BPL<sup>CH<sub>2</sub>SPh</sup> mediated by complex **1d** in the presence of *i*PrOH and precipitated twice in cold pentane (Table 1, entry 27) (\*: minor peaks correspond to the degradation product **3** of BPL<sup>CH<sub>2</sub>SPh</sup>).

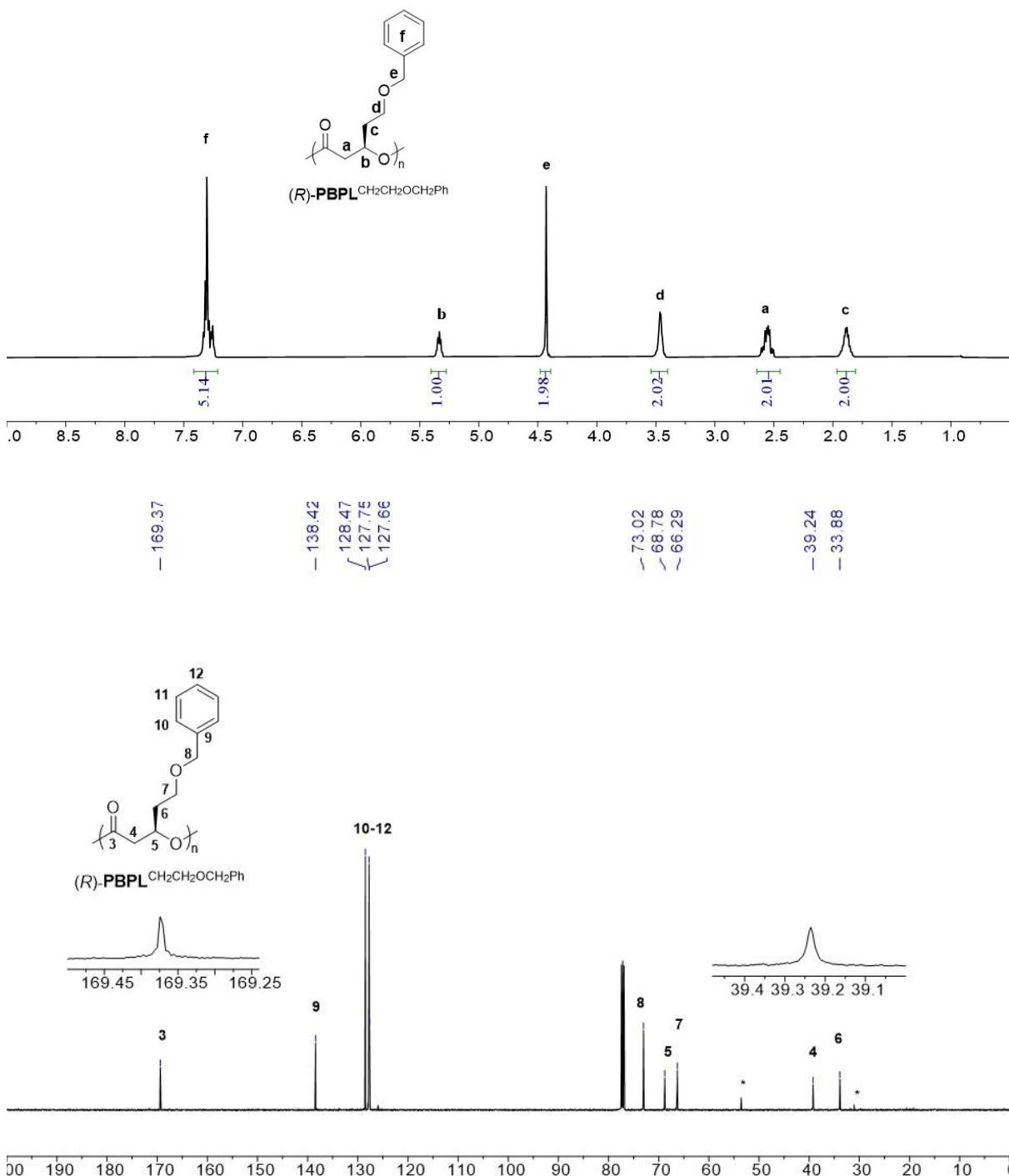


**Figure S14.**  $^1\text{H}$  (top) and  $^{13}\text{C}$  (bottom) NMR spectrum (500 and 125 MHz,  $\text{CDCl}_3$ , 25 °C) of *isotactic*  $\text{PBPL}^{\text{CH}_2\text{CH}_2\text{OCH}_2\text{Ph}}$  prepared from the ROP of  $(R)\text{-BPL}^{\text{CH}_2\text{CH}_2\text{OCH}_2\text{Ph}}$  mediated by complex **1d** in the presence of  $i\text{PrOH}$  and precipitated twice in cold pentane (Table 1, entry 40).

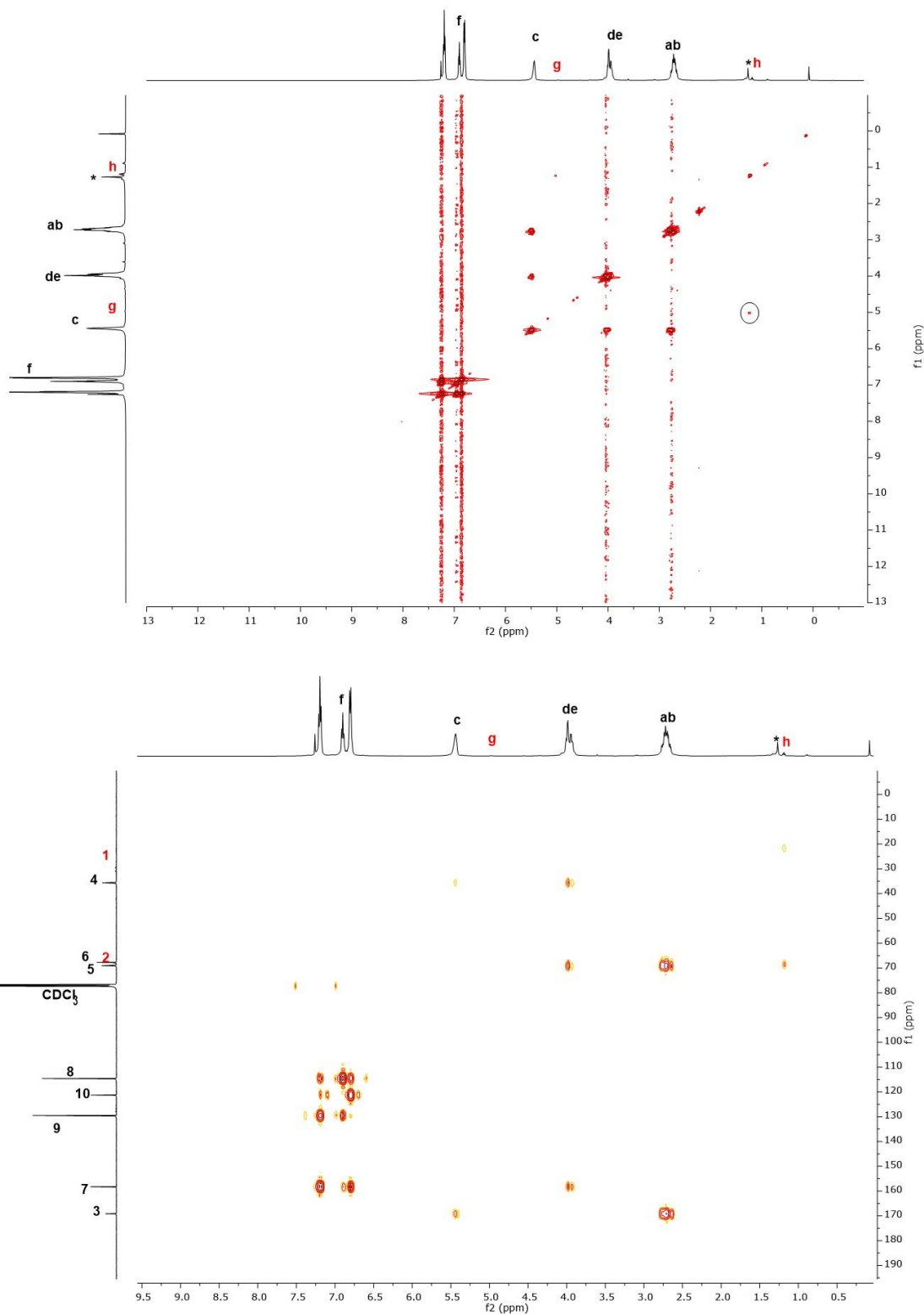


**Figure S15.** <sup>1</sup>H-<sup>1</sup>H COSY NMR spectrum (500 MHz, CDCl<sub>3</sub>, 25 °C) (top) and <sup>1</sup>H-<sup>13</sup>C HMBC (500 MHz, 125 MHz, CDCl<sub>3</sub>, 25 °C) (bottom) of syndiotactic PBPL-CH<sub>2</sub>OPh precipitated twice in cold pentane (Table 1, entry 6) (\*: residual H-grease).

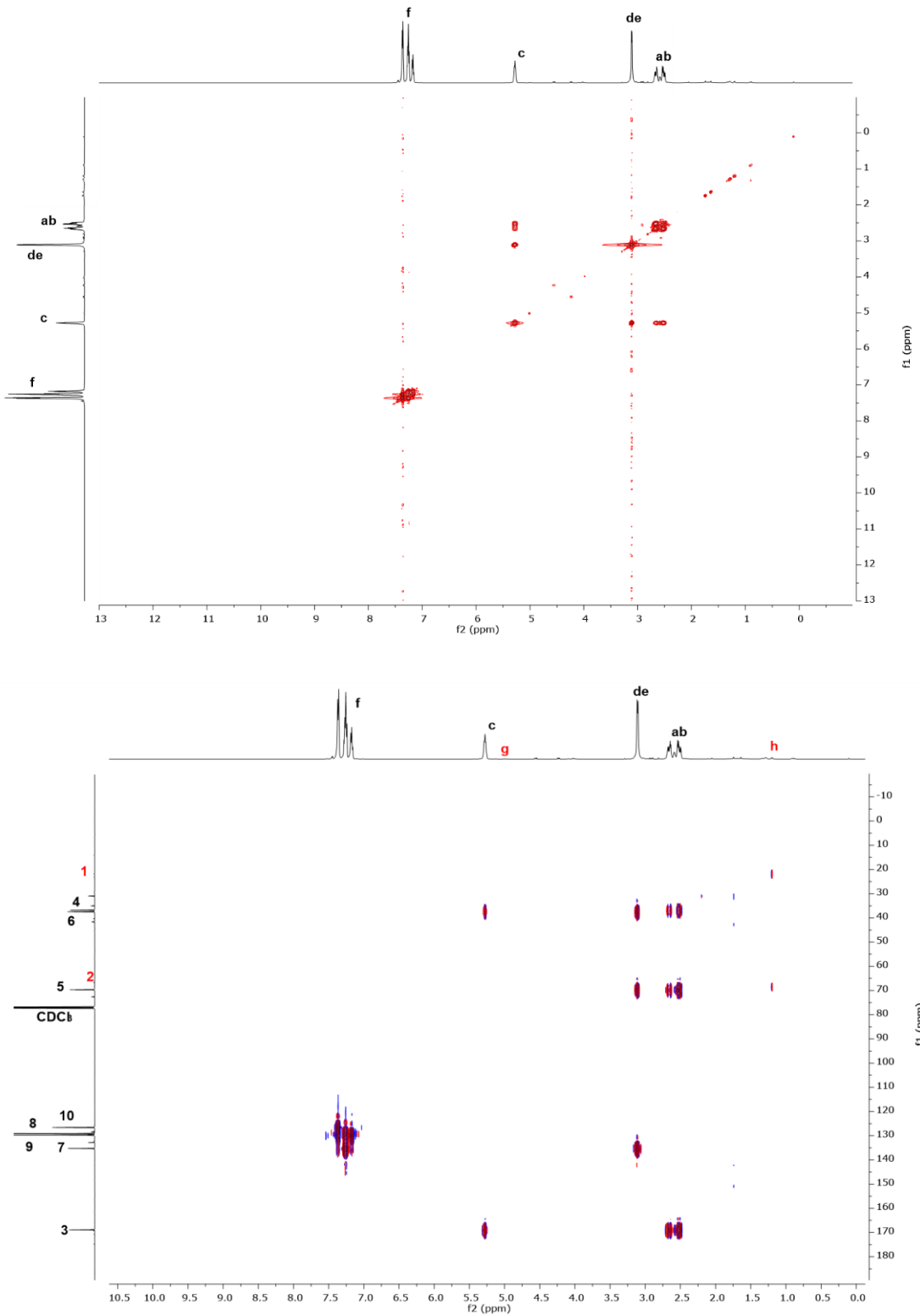


**Figure S16.** <sup>1</sup>H-<sup>1</sup>H COSY NMR spectrum (500 MHz, CDCl<sub>3</sub>, 25 °C) (top) and <sup>1</sup>H-<sup>13</sup>C HMBC (500 MHz, 125 MHz, CDCl<sub>3</sub>, 25 °C) (bottom) of syndiotactic PBPL<sup>CH2SPh</sup> precipitated twice in cold pentane (Table 1, entry 26).

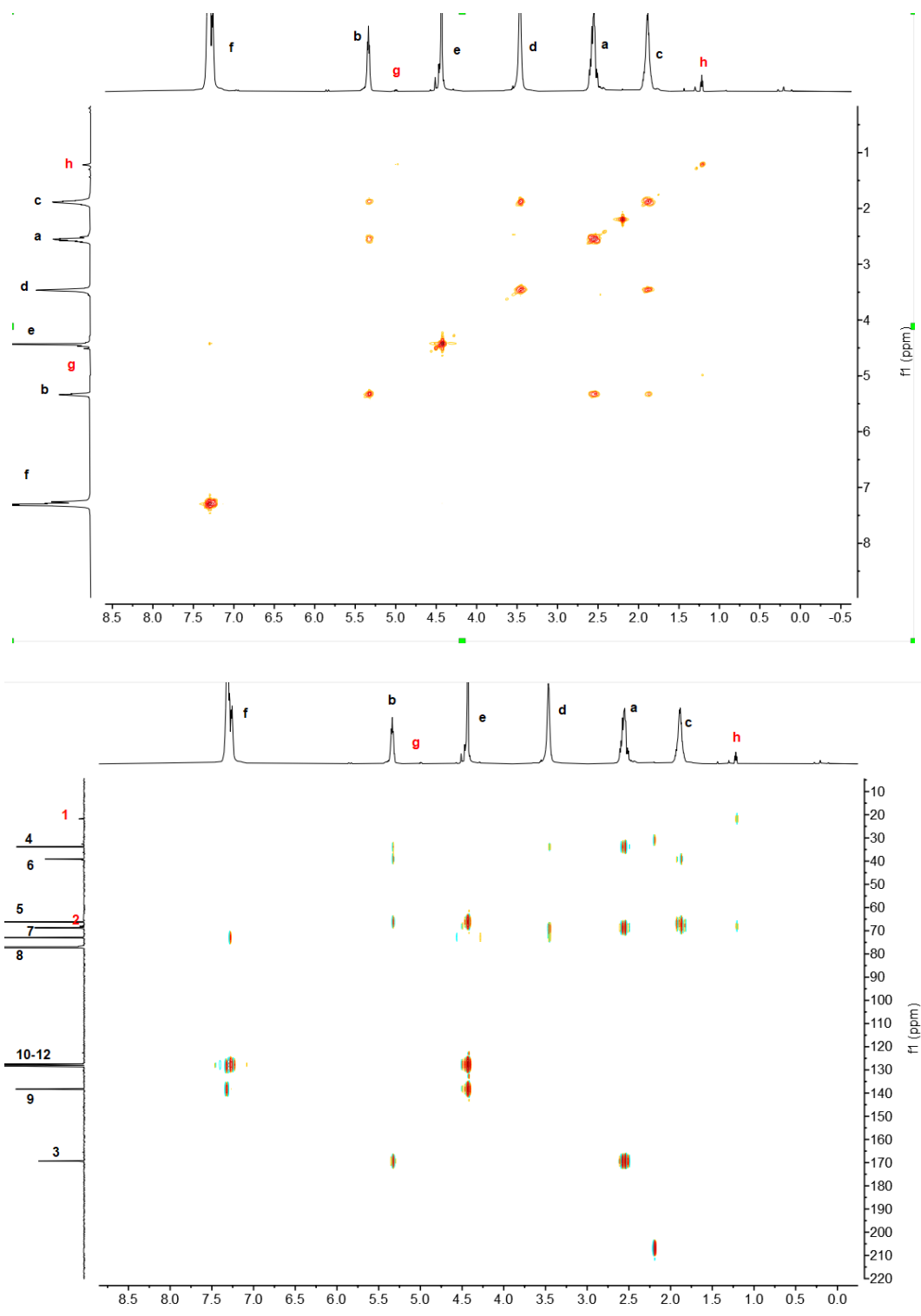


**Figure S17.**  $^1\text{H}$ - $^1\text{H}$  COSY NMR spectrum (500 MHz,  $\text{CDCl}_3$ , 25 °C) (top) and  $^1\text{H}$ - $^{13}\text{C}$  HMBC (500 MHz, 125 MHz,  $\text{CDCl}_3$ , 25 °C) (bottom) of syndiotactic PBPL- $\text{CH}_2\text{CH}_2\text{OCH}_2\text{Ph}$  precipitated twice in cold pentane (Table 1, entry 33).

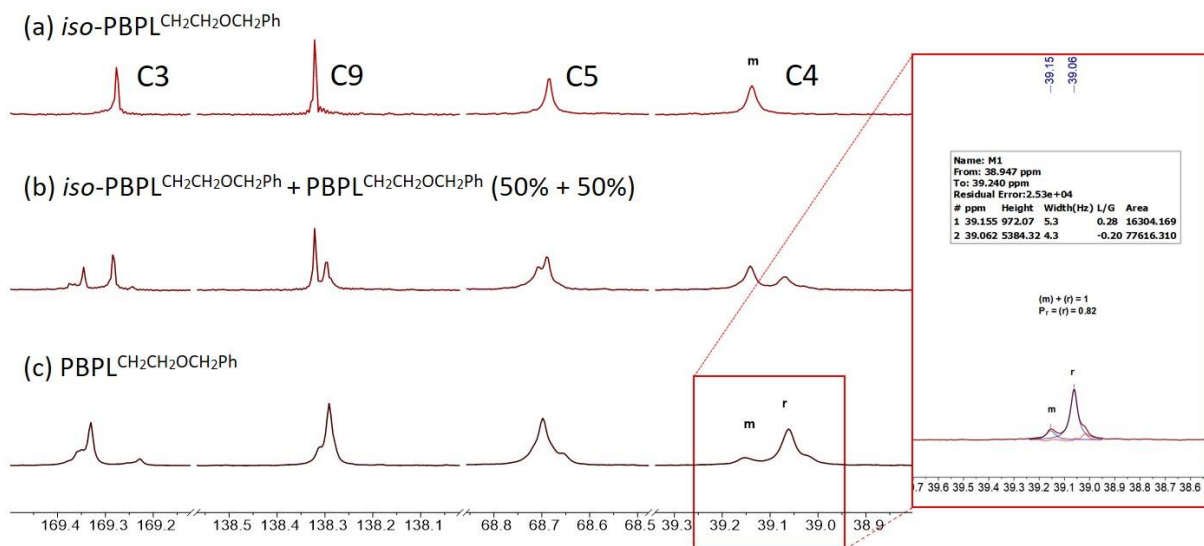


**Figure S18.** (a) Details of  $^{13}\text{C}$  NMR spectrum (125 MHz,  $\text{CDCl}_3$ ) of *isotactic*  $\text{PBPL}^{\text{CH}_2\text{CH}_2\text{OCH}_2\text{Ph}}$ ; (b) a blend of *isotactic*  $\text{PBPL}^{\text{CH}_2\text{CH}_2\text{OCH}_2\text{Ph}}$  and  $\text{PBPL}^{\text{CH}_2\text{CH}_2\text{OCH}_2\text{Ph}}$  (Table 1, entries 40,39); (c) Details of  $^{13}\text{C}$  NMR spectrum of  $\text{PBPL}^{\text{CH}_2\text{CH}_2\text{OCH}_2\text{Ph}}$  (Table 1, entry 39). The  $P_r$  values of  $\text{PBPL}^{\text{CH}_2\text{CH}_2\text{OCH}_2\text{Ph}}$  is then typically determined from the area fitting (or integration) values obtained from the NMR MestReNova software of the deconvoluted signals (labelled 1 and 2) corresponding to the *racemic* ( $r$ ) and *meso* ( $m$ ) diads, according to the equation:  $P_r = (P_r(\text{C}_3) + P_r(\text{C}_5) + P_r(\text{C}_4)) / 3$ , with  $P_r(\text{C}_x) = \text{Area } 1 / (\text{Area } 1 + \text{Area } 2)$  and  $\text{Cx}$  = corresponding carbon atom labeling.

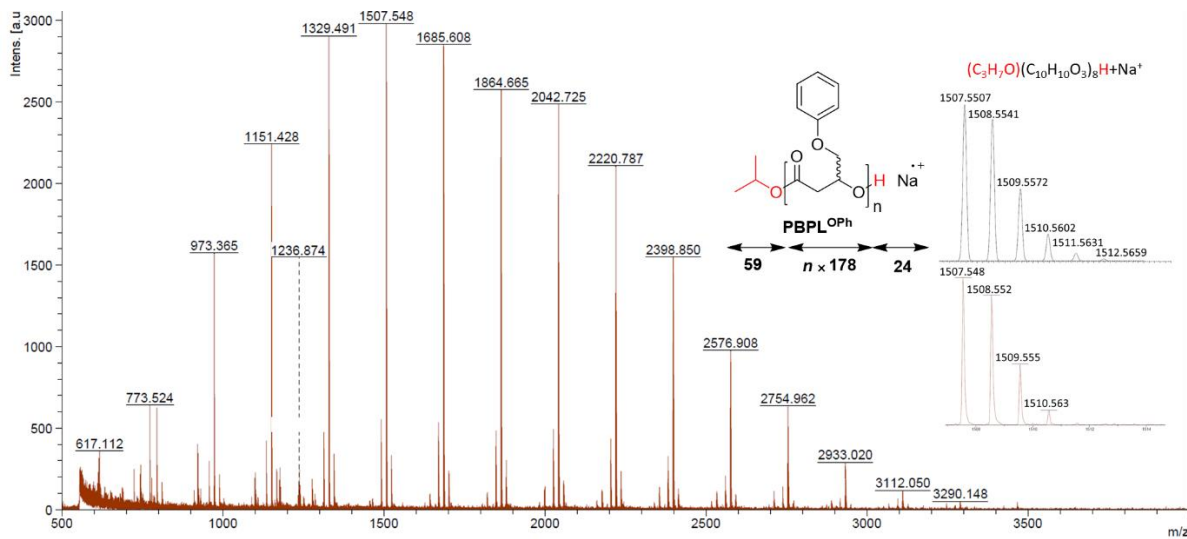


**Figure S19.** MALDI-ToF MS (DCTB matrix, ionized by  $\text{Na}^{+}$ ) of  $\text{PBPL}^{\text{CH}_2\text{OPh}}$  precipitated twice in cold pentane (Table 1, entry 5). Right zoomed regions correspond to the simulated (top) and experimental (bottom) spectra.

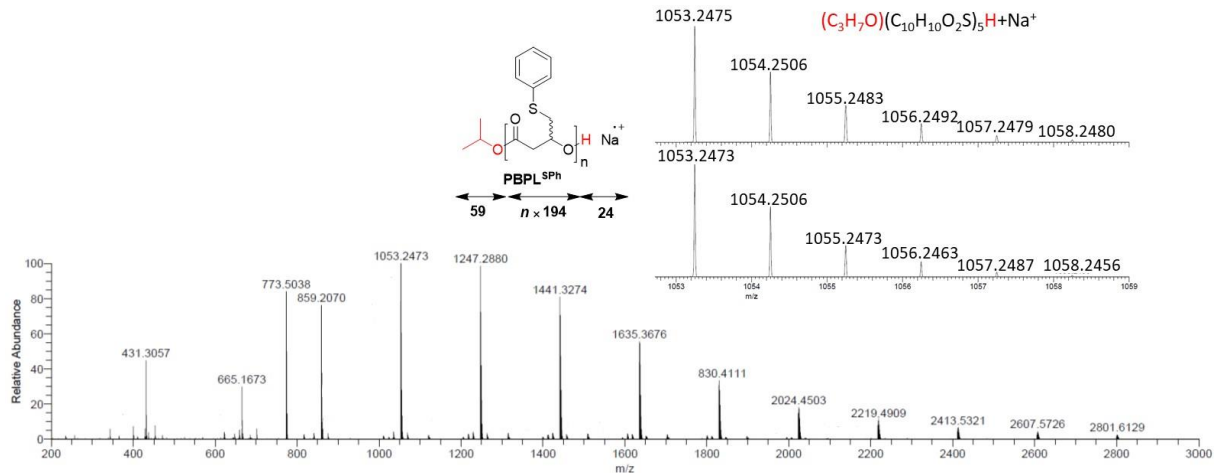


**Figure S20.** ESI-MS (ionized by  $\text{Na}^{+}$ , solvent  $\text{CH}_3\text{OH}/\text{CH}_2\text{Cl}_2$  (90/10 v:v) of  $\text{PBPL}^{\text{CH}_2\text{SPh}}$  (Table 1, entry 24) precipitated twice in cold pentane; right zoom spectra are theoretical data (top) vs. experimental (bottom).

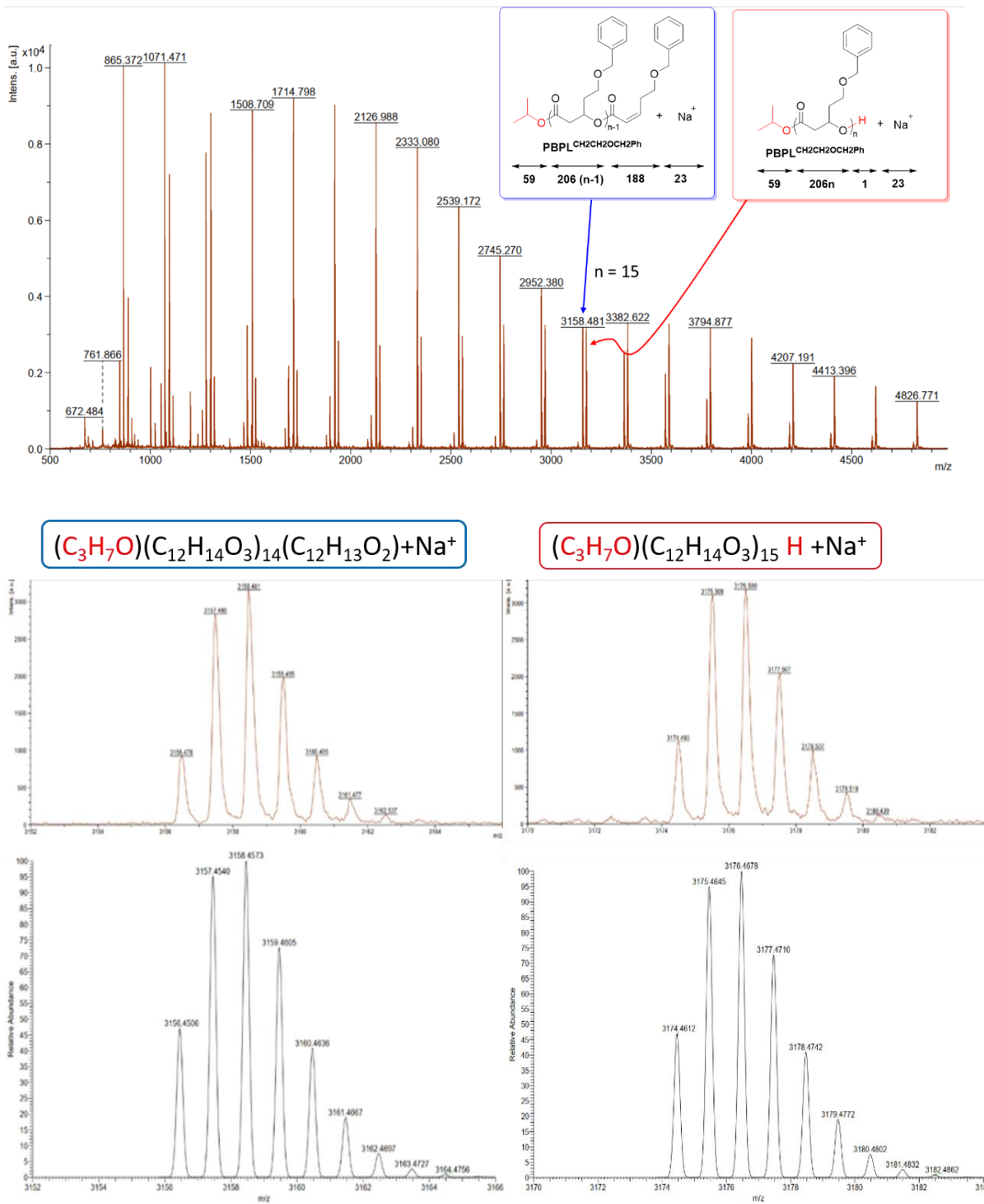


**Figure S21.** MALDI-ToF MS (DCTB matrix, ionized by  $\text{Na}^+$ ) of  $\text{PBPL}(\text{CH}_2\text{CH}_2\text{OCH}_2\text{Ph})$  precipitated twice in cold pentane (Table 1, entry 34). Zoomed regions correspond to the simulated (top) and experimental (bottom) spectra.

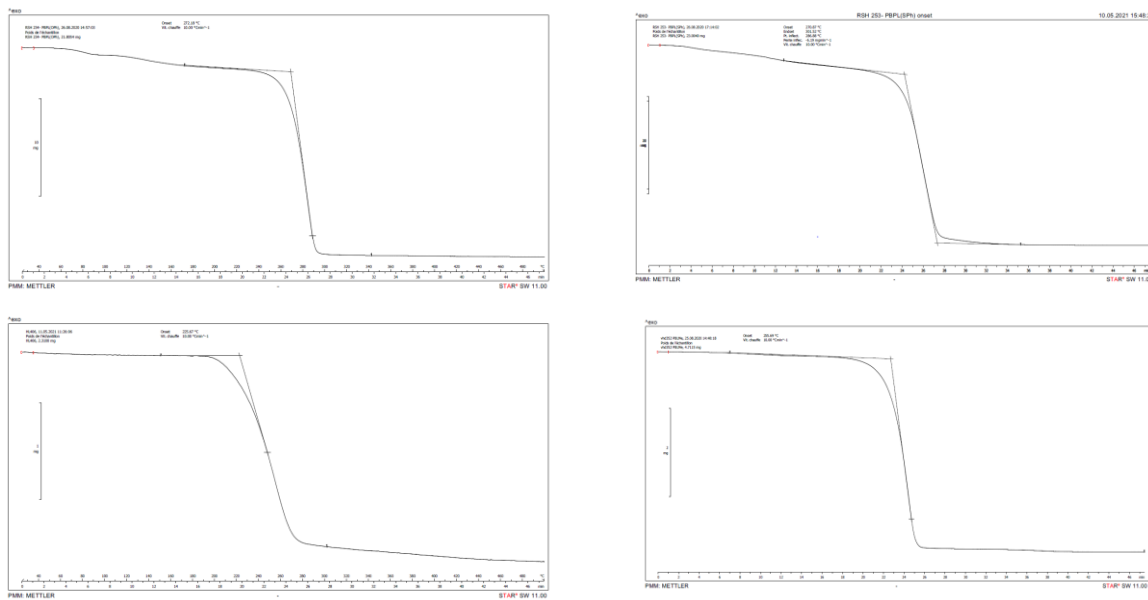


**Figure S22.** TGA thermograms of syndiotactic  $\text{PBPL}^{\text{CH2OPh}}$  (top-left) (Table 1, entry 7); syndiotactic  $\text{PBPL}^{\text{CH2SPh}}$  (top-right) (Table 1, entry 22); syndiotactic  $\text{PBPL}^{\text{CH2CH2OCH2Ph}}$  (bottom-left) (Table 1, entry 38); and (bottom right) for  $\text{PBPL}^{\text{Me}}$  ( $M_{\text{n,NMR}} = 7900 \text{ g mol}^{-1}$ ,  $D_{\text{M}} = 1.04$ ;  $P_{\text{r}} = 0.84$ ) prepared by ROP as previously reported (A. Amgoune, C. M. Thomas, S. Ilinca, T. Roisnel and J.-F. Carpentier, *Angew. Chem. Int. Ed.* 2006, **45**, 2782 –2784).

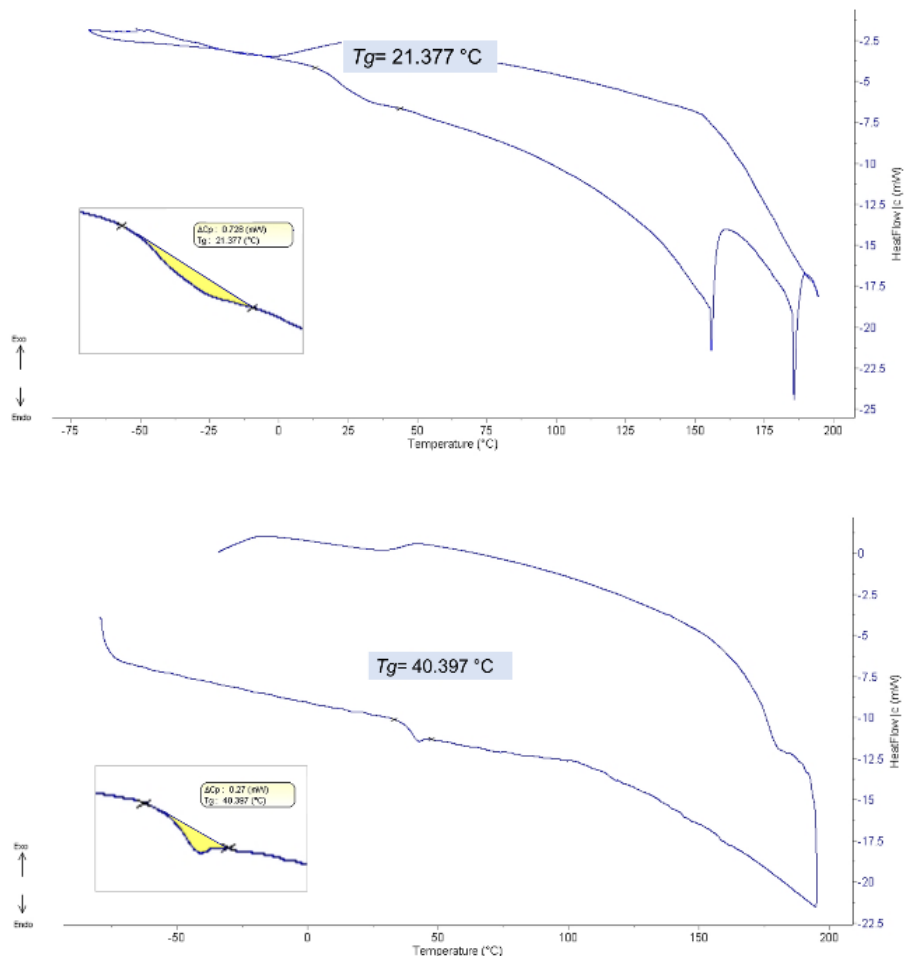


**Figure S23.** DSC thermogram (heating rate of  $10 \text{ } ^\circ\text{Cmin}^{-1}$ , second heating cycle, from  $-80$  to  $200 \text{ } ^\circ\text{C}$ ) of: (top) syndiotactic  $\text{PBPL}^{\text{CH2OPh}}$  ( $P_r 0.75$ ) synthesized by ROP of  $\text{rac-BPL}^{\text{CH2OPh}}$  with  $\text{Y}\{\text{ONNO}^{\text{Cl2}}\}/(\text{iPrOH})$  (Table 1, entry 4) - The spikes observed (ca  $160 \text{ } ^\circ\text{C}$ ,  $190 \text{ } ^\circ\text{C}$ ) arise from the cooling that sometimes occur upon filling in the liquid nitrogen fluid required to cool down the temperature; (bottom) syndiotactic  $\text{PBPL}^{\text{CH2OPh}}$  ( $P_r 0.83$ ) synthesized by ROP of  $\text{rac-BPL}^{\text{CH2OPh}}$  with  $\text{Y}\{\text{ONNO}^{\text{tBu2}}\}/(\text{iPrOH})$  (Table 1, entry 12).

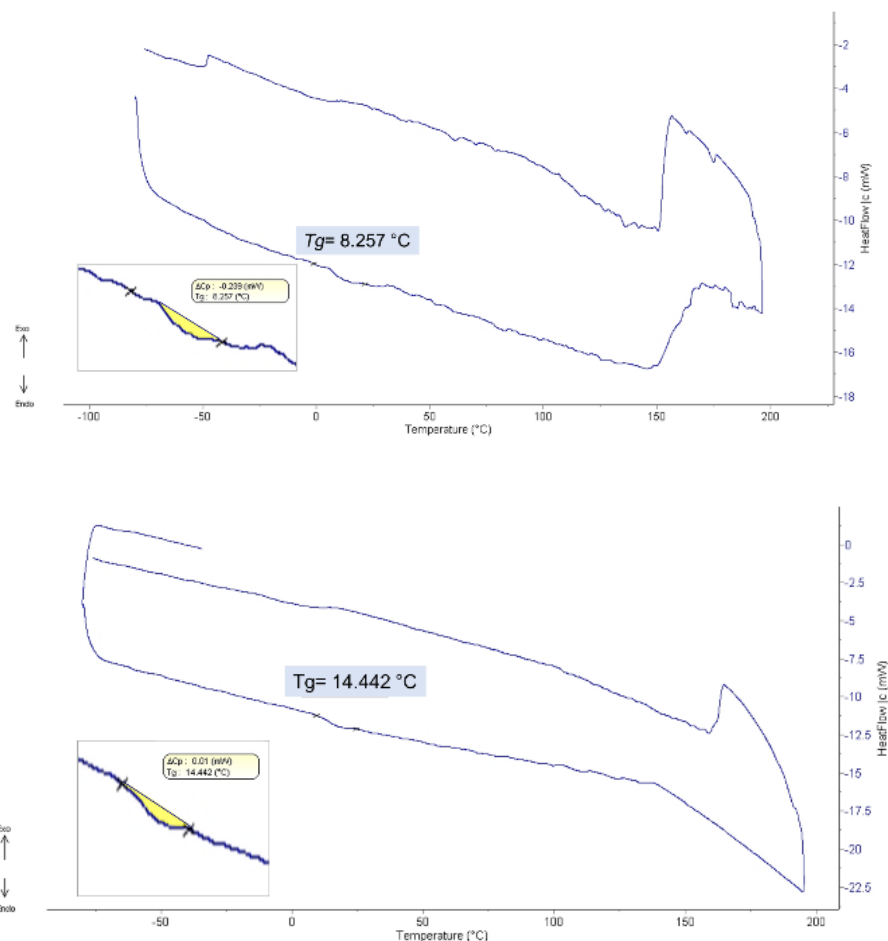


**Figure S24.** DSC thermogram (heating rate of  $10\text{ }^\circ\text{C min}^{-1}$ , second heating cycle  $-80$  to  $200\text{ }^\circ\text{C}$ ) of: (top) syndiotactic  $\text{PBPL}^{\text{CH2SPh}}$  ( $P_r 0.76$ ) synthesized by ROP of  $\text{rac-BPL}^{\text{CH2SPh}}$  with  $\text{Y}\{\text{ONNO}^{\text{Me}2}\}/(i\text{PrOH})$  (Table 1, entry 15); (bottom) syndiotactic  $\text{PBPL}^{\text{CH2SPh}}$  ( $P_r 0.86$ ) synthesized by ROP of  $\text{rac-BPL}^{\text{CH2SPh}}$  with  $\text{Y}\{\text{ONNO}^{\text{tBu}2}\}/(i\text{PrOH})$  (Table 1, entry 21).

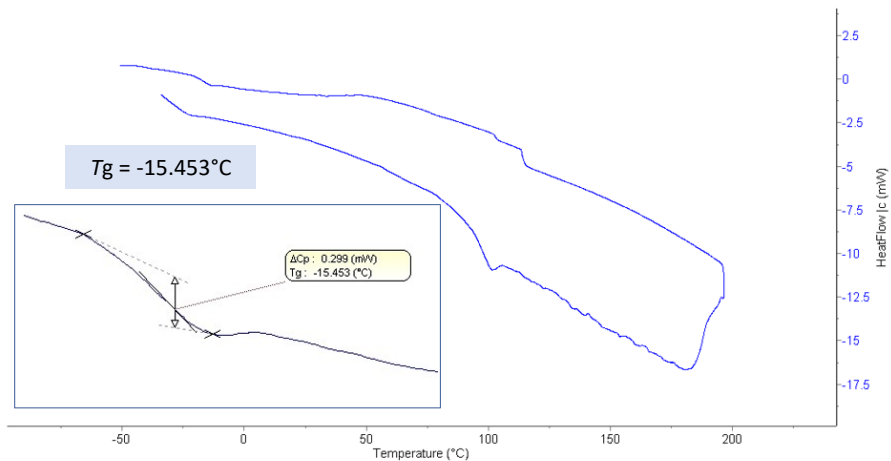
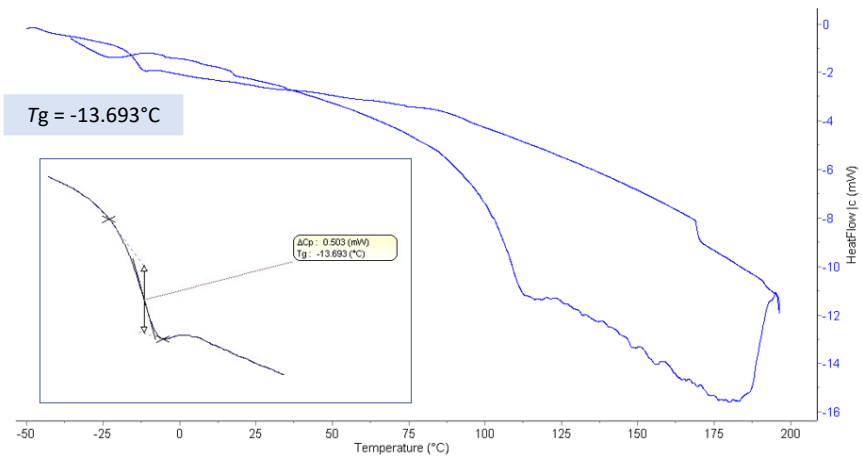


**Figure S25.** DSC thermogram (heating rate of  $10^\circ\text{Cmin}^{-1}$ , second heating cycle  $-60$  to  $200^\circ\text{C}$ ) of : (top) syndiotactic PBPL<sup>CH2CH2OCH2Ph</sup> ( $P_r$  0.86) synthesized by ROP of *rac*-BPL<sup>CH2CH2OCH2Ph</sup> with Y{ONNO<sup>cumyl2</sup>}/(iPrOH) (Table 1, entry 36); (bottom) atactic PBPL<sup>CH2CH2OCH2Ph</sup> ( $P_r$  0.49) synthesized by ROP of *rac*-BPL<sup>CH2CH2OCH2Ph</sup> with Y{ONNO<sup>Cl2</sup>}/(iPrOH) (Table 1, entry 31).